An inverse model to correct for the effects of post-depositional processing on ice-core nitrate and its isotopes: model framework and applications at Summit, Greenland and Dome C, Antarctica

Zhuang Jiang[1], Becky Alexander[2], Joel Savarino[3], Lei Geng[1,4,5*]

[1] Deep Space Exploration Laboratory/School of Earth and Space Sciences, University of Science and Technology of China, Hefei, Anhui, China

[2] Department of Atmospheric Sciences, University of Washington, Seattle WA, USA

[3] Univ. Grenoble Alpes, CNRS, IRD, G-INP, Institut des Géosciences de l'Environnement, Grenoble, France

[4] Laboratory for Ocean Dynamics and Climate, Pilot National Laboratory for Marine Science and Technology (Qingdao), Qingdao, Shandong, China

[5] CAS Center for Excellence in Comparative Planetology, University of Science and Technology of China, Hefei, Anhui, China

Correspondence to: Lei Geng (genglei@ustc.edu.cn)

Abstract

Comprehensive evaluation of the effects of post-depositional processing is a prerequisite for appropriately interpreting ice-core records of nitrate concentration and isotopes. In this study, we developed an inverse model that uses archived snow/ice-core nitrate signals to reconstruct primary nitrate flux (i.e., the deposition flux of nitrate to surface snow that originates from long-range transport or stratospheric input) and its isotopes (δ^{15}N and Δ^{17}O). The model was then applied to two polar sites, Summit, Greenland and Dome C, Antarctica using measured snowpack nitrate concentration and isotope profiles in the top few meters. At Summit, the model successfully reproduced the observed atmospheric δ^{15}N(NO$_3^-$) and Δ^{17}O(NO$_3^-$) and their seasonality. The model was also able to reasonably reproduce the observed snowpack nitrate profiles at Dome C as well as the skin layer and atmospheric δ^{15}N(NO$_3^-$) and Δ^{17}O(NO$_3^-$) at the annual scale. The calculated F_{pri} at Summit was 6.9×10^{-6} kgN m^2 a^{-1} and the calculated

$\Delta^{17}O(NO_3^-)$ of F_{pri} is consistent with atmospheric observations in the northern hemisphere. However, the calculated $\delta^{15}N(NO_3^-)$ of F_{pri} displays an opposite seasonal pattern to atmospheric observations in the northern mid-latitudes, but is consistent with observations in two Arctic coastal sites. The calculated F_{pri} at Dome C varies from 1.5

35   to 2.2 $\times 10^{-6}$ kgN m^{-2} a^{-1}, with $\delta^{15}N(NO_3^-)$ of F_{pri} varying from 6.2 to 29.3 ‰ and $\Delta^{17}O(NO_3^-)$ of F_{pri} varying from 48.8 to 52.6 ‰. The calculated F_{pri} at Dome C is close to the previous estimated stratospheric denitrification flux in Antarctica, and the high $\delta^{15}N(NO_3^-)$ and $\Delta^{17}O(NO_3^-)$ of F_{pri} at Dome C also point towards the dominate role of stratospheric origin of primary nitrate to Dome C.

1. Introduction

Nitrate ion (NO_3^-) is routinely measured in polar snow and ice cores. The precursor of atmospheric nitrate is nitrogen oxides NO_x (=$NO+NO_2$), which plays a fundamental role in the production of tropospheric ozone and interconversion of atmospheric HO_x

45   (= OH + HO_2) radicals (Seinfeld et al., 1998; Sillman, 1999). Given the potential link between ice-core nitrate and atmospheric NO_x, some previous studies proposed that ice-core nitrate records could be used to derive information regarding past atmospheric NO_x abundance (Dibb et al., 1998; Röthlisberger et al., 2000). In addition, the oxygen isotope mass-independent fractionation signal ($\Delta^{17}O = \delta^{17}O - 0.52 \times \delta^{18}O$) of nitrate is a reliable

50   proxy of atmospheric O_3/HO_x ratio and is directly related to atmospheric oxidizing environment (Alexander et al., 2004; Alexander et al., 2015; Geng et al., 2017; Sofen et al., 2014). These unique features render ice core nitrate a potentially useful proxy to retrieve information on atmospheric oxidation environment in the past (Alexander et al., 2015).

55   Interpretations of ice-core nitrate records are, however, not straightforward (Wolff et al., 2008). Unlike other less reactive species in ice cores such as sulfate, ice-core nitrate may not be able to directly track its atmospheric abundance (Iizuka et al., 2018). To link ice-core nitrate to atmospheric NO_x abundance, other information including the conversion rate of NO_x to nitrate, the mean lifetime of atmospheric nitrate, and the

60 impact of post-depositional processing must be considered (Wolff, 1995; Wolff et al., 2008). Among these factors, the post-depositional processing of snow nitrate is the first gap in linking ice-core nitrate to atmospheric nitrate and/or NO_x.

Snow nitrate is reactive under exposure to sunlight and can be photolyzed to form NO_x and HONO (Honrath et al., 2002; Chu and Anastasio, 2003), which is rapidly
65 transported to the overlying atmosphere via diffusion and convection (Zatko et al., 2013). These photoproducts subsequently reform nitrate (i.e., we further refer to this as snow-sourced nitrate) and which is redeposited locally or be exported away, leading to a recycling of nitrate at the air-snow interface (Erbland et al., 2013; Frey et al., 2009). The reformed nitrate would inherit $\Delta^{17}O$ signals under local oxidation conditions that
70 is different from primary nitrate, and the re-deposition of atmospheric nitrate could also result in nitrogen isotopic fractionation depending on the different deposition mechanisms (Erbland et al., 2013; Jiang et al., 2022). This post-depositional processing not only disturbs the link between nitrate in snow and its atmospheric precursors but also alters its isotopic signals (Erbland et al., 2013; Jiang et al., 2021; Jiang et al., 2022;
75 Shi et al., 2015). But since these processes are initiated by sunlight, the post-depositional processing is muted in polar winter when sunlight is absent.

It is expected that the degree of post-depositional processing varies with changes in factors such as snow accumulation rate under different climates (Akers et al., 2022; Geng et al., 2015), causing corresponding shifts in the preserved nitrate signals. For
80 example, the lower snow accumulation rate in glacial times would favor a higher degree of post-depositional processing with elevated $\delta^{15}N(NO_3^-)$ relative to the Holocene as reflected by the GISP2 ice-core records (Geng et al., 2015; Hastings et al., 2005). Moreover, both observational and modeling studies have suggested that at sites with relatively high snow accumulation rates such as Summit, Greenland, the post-
85 depositional processing of snow nitrate under present day conditions also has a significant impact on seasonal $\delta^{15}N(NO_3^-)$ variations, although its integral effects at the annual scale are limited (Jiang et al., 2021; Jiang et al., 2022). In addition, the $\Delta^{17}O$ of snow nitrate would also be altered via secondary chemistry during photolysis on snow

grain (i.e., the cage effect) and this effect is enhanced with lower snow accumulation rates (Erbland et al., 2013; Frey et al., 2009; Mccabe et al., 2005; Meusinger et al., 2014). Thus, it is critical to evaluate the impact of post-depositional processing on ice core nitrate records before interpretation, especially for records covering different climates with changes in snow accumulation rates.

Primary nitrate to the polar ice sheets mainly originates from midlatitudes via long-range transport and with extra contributions from stratospheric input (Lee et al., 2014; Legrand and Delmas, 1986; Fischer et al., 1998; Savarino et al., 2007). To build the link between ice-core and atmospheric nitrate, Geng et al. (2015) proposed a simple method of using $\delta^{15}N(NO_3^-)$ to estimate the fractional loss of snow nitrate caused by post-depositional processing. This method takes advantage of the high sensitivity of $\delta^{15}N(NO_3^-)$ to the degree of photolytic loss (Erbland et al., 2013; Frey et al., 2009). If $\delta^{15}N$ of the initially deposited nitrate can be assumed, the residual fraction of snow nitrate can be calculated by applying a Rayleigh type isotope fractionation model. The photolysis fractionation constant ($^{15}\varepsilon_p$) can be estimated via the prescribed actinic flux spectrum and the absorption cross section for different nitrate isotopologues (Berhanu et al., 2014). Based on this method, Geng et al. (2015) estimated that as much as 45-53% of snow nitrate was lost after deposition during the last glacial time in the GISP2 ice core record. However, it's difficult to justify the assumed $\delta^{15}N$ of deposited nitrate under different climates, and the method cannot correct for post-depositional modification of $\Delta^{17}O(NO_3^-)$.

Erbland et al. (2015) developed a 1-D snow photochemistry model (TRANSITS, https://github.com/JZxxhh/TRANSITS-model, last access: 29 January 2024) that quantifies the effects of post-depositional processing on the preservations of nitrate and its isotopes in ice cores. The model comprises a series of physicochemical processes, including UV photolysis of snow nitrate, emission of NO_x to the overlying atmosphere, local oxidation and nitrate deposition. In addition, changes in the isotopic composition of nitrate ($\delta^{15}N$ and $\Delta^{17}O$) at each step of the post-depositional processing are also explicitly incorporated. Recently, Shi et al. (2023) extended or followed the TRANSITS

model framework to include snowpack $\delta^{18}O(NO_3^-)$ simulation during the preservation of nitrate in snow. The latter was built upon the same chemical processes related to modeling $\Delta^{17}O(NO_3^-)$ changes during the post-depositional processing. However, the fractionation factor of $\delta^{18}O$ during snow nitrate photolysis ($^{18}\varepsilon_p$) had to be scaled to reproduce the observations. In this case it remains unclear why the theoretical fractionation factor calculated using the ZPE (zero-point energy) shifted method (Frey et al., 2009) works well on $\delta^{15}N(NO_3^-)$ but not on $\delta^{18}O(NO_3^-)$. Nevertheless, the uncertainties associated with $\delta^{18}O$ fractionations during snow nitrate photolysis and other processes (e.g., the cage effect, reformation of nitrate from NO_2, etc.) make this simulation less useful and reliable than for $\Delta^{17}O(NO_3^-)$, for which there are much fewer influencing factors and are easier to constrain. The TRANSITS model has been applied in various locations with different snow accumulation rates and well reproduced the observed snowpack nitrate and isotope profiles (Erbland et al., 2015; Jiang et al., 2021; Winton et al., 2020; Zatko et al., 2016). Based on model sensitivity tests, Erbland et al. (2015) proposed a framework to correct for the effects of post-depositional processing and to retrieve atmospheric information related to F_{pri} at Dome C. However, the framework is rather complicated, and it assumes $\delta^{15}N$ of the archived nitrate is exclusively determined by the degree of nitrate post-depositional processing. Therefore, the framework cannot be applied to sites with moderate or high snow accumulation rates such as WAIS Divide, Antarctica and Summit, Greenland, where factors other than post-depositional processing may also contribute to $\delta^{15}N$ variations across different periods and/or climates (Hastings et al., 2005; Jiang et al., 2021).

In summary, TRANSITS is a forward model, and it requires prior knowledge of the distribution (e.g., weekly or monthly) of primary nitrate flux and isotopes as model inputs, which is usually unavailable due to the lack of direct observations. In this study, we developed an inverse modeling framework (i.e., the inverse of the TRANISTS model) that uses snowpack and/or ice-core preserved nitrate signals (concentrations and isotopes) as model inputs, and properties of primary nitrate including its flux and isotopes ($\delta^{15}N$ and $\Delta^{17}O$) can be directly retrieved with constraints from snow

accumulation rate and other known parameters (e.g., snow physicochemical properties). We assessed the model with observations at Summit, Greenland and Dome C, Antarctica, two representative sites with approximately the high-end and low-end snow accumulation rates at present day conditions.

2. Model description

Table 1. List of major parameters used in the inverse model.

Compartment	Parameter	Unit	Definition
Input (could be obtained from measurements)	FA	kgN m^{-2} a^{-1}	Archived nitrate flux
	δ^{15}N(FA)	‰	δ^{15}N of archived nitrate ~~flux~~
	Δ^{17}O(FA)	‰	Δ^{17}O of archived nitrate ~~flux~~
	A	kg m^{-2} a^{-1}	Snow accumulation rate
	ρ	kg m^{-3}	Snow density
	TCO	DU	Total column ozone
	LAI[a]	ng g^{-1}	Light absorption impurities
	Φ	Dimensionless	Quantum yield of nitrate photolysis
	σ	cm^{-2}	Absorption cross section for NO_3^-
Input (constrained by observations)	ε_d	‰	Nitrogen isotope fractionation factor for nitrate deposition
	Δ^{17}O(FP)	‰	Δ^{17}O of photolytic nitrate ~~flux~~
	f_c	Dimensionless	Cage effect factor
	f_{exp}	Dimensionless	Exported nitrate factor
Model output	F$_{pri}$	kgN m^{-2} a^{-1}	Primary nitrate flux
	δ^{15}N(F$_{pri}$)	‰	δ^{15}N of primary nitrate ~~flux~~
	Δ^{17}O(F$_{pri}$)	‰	Δ^{17}O of primary nitrate ~~flux~~
	FD	kgN m^{-2} a^{-1}	Deposition nitrate flux
	δ^{15}N(FD)	‰	δ^{15}N of deposition nitrate ~~flux~~
	Δ^{17}O(FD)	‰	Δ^{17}O of deposition nitrate ~~flux~~
	FP	kgN m^{-2} a^{-1} / ‰	Photolytic nitrate flux
	δ^{15}N(FP)	‰	δ^{15}N of photolytic nitrate ~~flux~~
	δ^{15}N(NO$_3^-$)$_a$	‰	δ^{15}N of local atmospheric nitrate
	Δ^{17}O(NO$_3^-$)$_a$	‰	Δ^{17}O of local atmospheric nitrate

[a]Three types of light absorption impurity are considered in the inverse mode: black carbon, mineral dust and organic humic-like substance (HULIS).

The inverse model is designed based on the framework of the TRANSITS model but in an opposite direction of operating flows. The principle of the inverse model is that the archived snow nitrate concentration and isotope profiles from measurements are treated as model input, and they evolve inversely over time through the snow photic

160   zone (defined as 3 times of the snow e-folding depth where the radiation decreases to
        $1/e$ of its initial intensity at snow surface) to recover their initial states at the time of
        deposition , thus providing the initial isotope compositions and deposition fluxes before
        being affected by any post-depositional effects. The primary nitrate flux and its isotopes
        can be further obtained by solving the mass balance equations in the atmosphere box.

165   A schematic view of the inverse model is shown in Fig. 1 with arrows pointing toward
        the model direction flow (i.e. inverse of the real physical processes). Major parameters
        in the inverse model and their definitions are listed in Table 1.
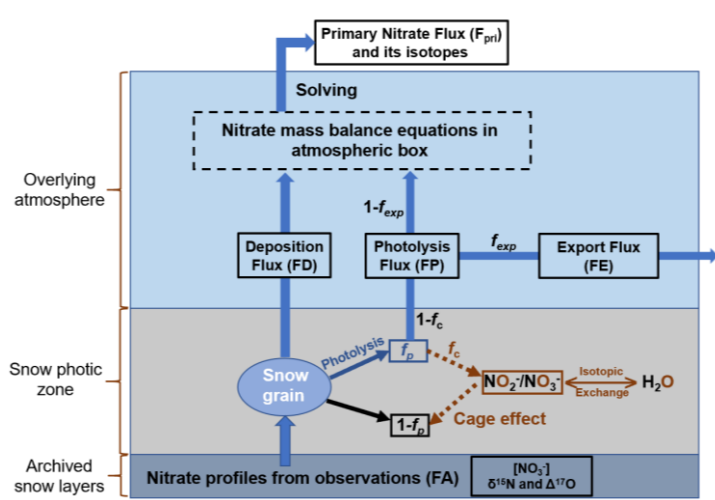
Figure 1. Schematic plot of the model domains of the inverse model including the
170   atmospheric box, the snow photic zone and the archived snow layers, where f_{exp}
        represents the fraction of nitrate exported from the site of photolysis. The nitrate
        isotopic and mass balance relationships on snow grains during photolysis are also
        shown, where f_p represents the fraction of snow nitrate being photolyzed, and f_c
        represents the fraction of photolyzed nitrate experiencing the cage effect (i.e.,
175   exchange of oxygen isotopes with snow water). FA represents the archived nitrate
        flux.

        The inverse model inherits most of the original processes and features in
        TRANSITS but with several modifications. In accordance with the TRANSITS model,
        the domains of the inverse model are represented by a 1-D atmosphere and snow
180   column. As shown in Fig. 1, the model contains three vertical parts, including the
        overlying atmospheric boundary layer which is treated as a single well-mixed box, and

the underlying snowpack which is further separated into a snow photic zone and the archived snow layers beneath the photic zone. The model time step is set to be one week by default. During each time step, the mass conservation equations in the atmospheric box are represented as follows:

$$\frac{dm_a}{dt} = F_{pri} + FP - FE - FD \tag{1}$$

$$\frac{d(m_a \times \delta^{15}N_a)}{dt} = F_{pri} \times \delta^{15}N(F_{pri}) + FP \times \delta^{15}N(FP) -$$
$$FE \times \delta^{15}N(FP) - FD \times \delta^{15}N(FD) \tag{2}$$

$$\frac{d(m_a \times \Delta^{17}O_a)}{dt} = F_{pri} \times \Delta^{17}O(F_{pri}) + FP \times \Delta^{17}O(FP) -$$
$$FE \times \Delta^{17}O(FE) - FD \times \Delta^{17}O(FD) \tag{3}$$

where the subscript "a" represents the atmospheric box, i.e., m_a refers to the mass of atmospheric nitrate, and $\delta^{15}N_a$ and $\Delta^{17}O_a$ refer to $\delta^{15}N$ and $\Delta^{17}O$ of atmospheric nitrate, respectively. Different nitrate fluxes transported in and out of the atmospheric box are denoted as FP, FE, and FD, where FP refers to the photolytic nitrate flux (the snow-sourced nitrate), FD refers to the atmospheric deposition nitrate flux, and FE refers to the exported nitrate flux that is horizontally transported out of the atmospheric box via air flow. Following Erbland et al. (2015), FE is assumed to be a portion (f_{exp}) of FP (i.e., FE = $f_{exp} \times$ FP) and maintains the isotopic signatures of FP.

In Eq. (1-3), the LHS (left-hand side) terms are two to three orders of magnitude smaller than nitrate fluxes in and out of the atmospheric box. Erbland et al. (2015) showed that the atmospheric nitrate mass was a factor of ~10^{-3} smaller than the surface snow nitrate reservoir at Dome C, and similar results were also found at Summit in Jiang et al. (2021). Thus, d(x)/dt is assumed to be zero at each time step (i.e. species and isotope compositions in the atmosphere are considered at steady state), which leads to simplified formulas for calculating F_{pri} via Eq. (4-6) as follows:

$$F_{pri} \approx FD - FP(1 - f_{exp}) \tag{4}$$

$$\delta^{15}N(F_{pri}) \approx \frac{FD \times \delta^{15}N(FD) - FP \times (1 - f_{exp}) \times \delta^{15}N(FP)}{FD - FP \times (1 - f_{exp})} \tag{5}$$

$$\Delta^{17}O(F_{pri}) \approx \frac{FD \times \Delta^{17}O(FD) - FP \times (1 - f_{exp}) \times \Delta^{17}O(FP)}{FD - FP \times (1 - f_{exp})} \tag{6}$$

Hence, if the magnitude and isotopic compositions of FP and FD in each time step are known, F_{pri} can be calculated. FP and FD are calculated from the inverse evolution of snowpack nitrate are described in the following sections.

2.1 The backward evolution of snowpack nitrate

Starting with an arbitrary snowpack nitrate depth profile at a given time step, changes in nitrate concentration and isotopic compositions ($\delta^{15}N$ and $\Delta^{17}O$) in a certain snow layer in the photic zone induced by photolysis can be calculated as follows:

$$c(SN_n') = \frac{c(SN_n)}{(1 - f_p) + f_c f_p} \tag{7}$$

$$\delta^{15}N(SN_n') = \delta^{15}N(SN_n) - \frac{(1 - f_p)(1 - f_c)\overline{\varepsilon_p}ln(1 - f_p)}{(1 - f_p) + f_c f_p} \tag{8}$$

$$\Delta^{17}O(SN_n') = \Delta^{17}O(SN_n)\frac{(1 - f_p) + f_c f_p}{(1 - f_p) + \frac{2}{3}f_c f_p} \tag{9}$$

where c represent the nitrate concentration and SN_n refers to the nth snowpack layer, respectively, and the quotation mark in superscript refers to the initial state before being photolyzed at each time step. These equations are based on the nitrate mass and isotopic balances on snow grains during photolysis as shown in Fig. 1, and detailed derivations of these equations can be found in Appendix A.

In Eq (7-9), f_p represents the fraction of snow nitrate that undergoes photolysis at each time step, and f_c represents the fraction of nitrate photolysis intermediate undergoing the cage effect (Meusinger et al., 2014) which leads to apparent oxygen isotope exchange with water and lowers $\Delta^{17}O$ by a factor of 2/3. The potential isotope effect on $\delta^{15}N$ during cage effect remains unknown and is not considered. The value of f_p is calculated by the first-order reaction of nitrate photolysis:

$$f_p = 1 - \exp\left(-\int_0^{dt} J(t,z)dt\right) \tag{10}$$

where J represents the rate constant of nitrate photolysis that varies with time and depth of the snow layer. J is calculated from actinic flux (I), the quantum yield (Φ), and the absorption cross section (σ) of nitrate photolysis as follows:

$$J(t,z) = \int_{280\,nm}^{350\,nm} \Phi(\lambda) \times \sigma_{NO_3^-}(\lambda) \times I(z,\lambda)\, d\lambda \qquad (11)$$

The rate constant of $^{15}NO_3^-$ photolysis (J^*) is also calculated from the absorption cross section of the heavy isotopologue from Berhanu et al. (2014), and the photolysis fractionation constant for nitrogen isotope ε_p is calculated via:

$$\varepsilon_p(t,z) = \frac{J^*(t,z)}{J(t,z)} - 1 \qquad (12)$$

The solar zenith angle changes with time during each time step, leading to changes in the spectrum of actinic flux and subsequently changes in ε_p. To simplify the calculation, in Eq. (8) $\overline{\varepsilon_p}$ in a certain week is calculated by the weighted average of nitrogen isotope fractionation constant over the durations of different solar zenith angles (0-90 degree)~~in Eq. (8) the weighted average of nitrogen isotope fractionation constant ($\overline{\varepsilon_p}$) over durations in different solar zenith angle is used~~. The radiative transfer in snowpack is calculated using the parameterization from Zatko et al. (2013) to achieve fast online calculations, and this parameterization has been shown to be capable of providing consistent results with a high-order snowpack radiative transfer model DISORT (Zatko et al., 2013). The upper boundary conditions for the parameterization, i.e., the direct and diffuse components of the irradiance at the snow surface, are calculated offline using the Troposphere Ultraviolet and Visible (TUV) radiation model (Madronich et al., 1998) at different total column ozone (TCO) and solar zenith angle conditions.

The relationships between $c(SN_n)$, $\delta^{15}N(SN_n)$, $\Delta^{17}O(SN_n)$ and $c(SN_n{}')$, $\delta^{15}N(SN_n{}')$, $\Delta^{17}O(SN_n{}')$ in the snowpack are illustrated in Fig. 2, where $c(SN_n)$, $\delta^{15}N(SN_n)$, $\Delta^{17}O(SN_n)$ are the values after photolysis in the nth layer at a certain time step, and $c(SN_n{}')$, $\delta^{15}N(SN_n{}')$, $\Delta^{17}O(SN_n{}')$ are the values before photolysis (calculated by Eq (7-9)) and are also the values after photolysis in the prior time step when it was in the $(n-1)^{th}$ layer. By repeating this operation, the initially deposited values of nitrate concentration and isotopes for a given snow layer without influence from the photo-driven post-depositional processing (i.e., when this layer was at the surface) can be calculated, which is be further linked to FD.
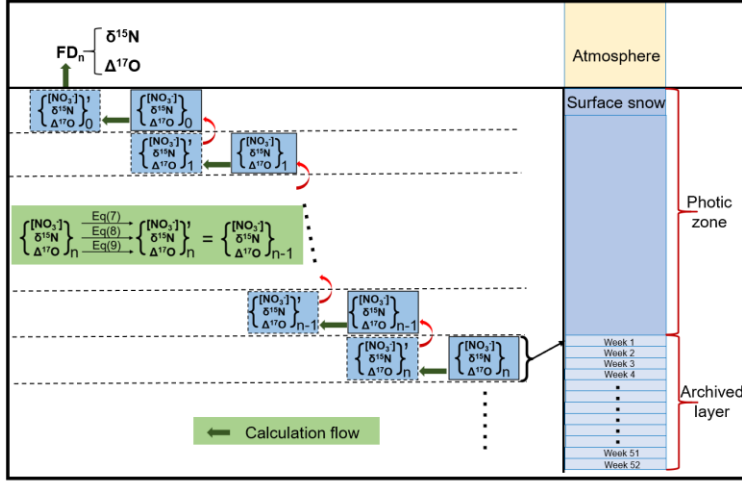
260

Figure 2. Schematic of the evolution of snowpack nitrate from the archived layer to its initial state at the snow surface. The quotation mark in the superscript of the bracket represents the status of snow nitrate before photolysis at each time step.

2.2 Determinations of FP and FD

265   FP and FD are determined during the inverse evolution of snowpack nitrate profiles. As shown in Fig. 1, photolytic nitrate flux and its $\delta^{15}N$ from the nth snow layer can be calculated via the mass balance relationships:

$$FP_n = c(SN'_n)f_p(1 - f_c)\rho_{snow}d_n/\Delta t \qquad (13)$$

$$\delta^{15}N(FP_n) = \delta^{15}N(SN_n) - \frac{\bar{\varepsilon_p}(1 - f_p)ln(1 - f_p)}{f_p} \qquad (14)$$

270   In Eq (13), ρ_{snow} is the density of snow, d_n is the thickness of the nth snow layer, which is equal to the accumulated snow thickness at one time step, and Δt is the default model time step (1 week). Eq (14) implicitly assumes that the reformed nitrate in the overlying atmosphere keeps the same $\delta^{15}N$ signals of the snow-emitted photoproduct of NO_2 because of isotope mass balance, i.e., essentially all NO_2 is oxidized into nitrate

275   at one time step. FP emitted from the whole snowpack and its $\delta^{15}N$ can be calculated by:

$$FP = \sum FP_n \qquad (15)$$

$$\delta^{15}N(FP) = \frac{\sum FP_n * \delta^{15}N(FP_n)}{\sum FP_n} \qquad (16)$$

For $\Delta^{17}O$ of FP, extra knowledge of the oxidizing agent concentrations in the local atmosphere including HO_2, RO_2 and O_3 must be provided (Appendix B). This is because the emitted NO_x would achieve photochemical steady state rapidly, thus erasing any original $\Delta^{17}O$ signal inherited from the snowpack nitrate. During the subsequent oxidation of atmospheric NO_2, one more oxygen atom inherited from the oxidants (e.g., OH or BrO) is incorporated into one newly formed HNO_3 molecule. Thus, $\Delta^{17}(FP)$ can be represented by 2/3 of $\Delta^{17}O(NO_2)$ plus 1/3 of $\Delta^{17}O(oxidant)$.~~The subsequent conversion of NO_2 to nitrate would also determine 1/3 of the oxygen atom of the newly formed nitrate.~~

FD and its isotopic signals can be obtained from the uppermost snow layer before photolysis occurs as illustrated in Fig.2:

$$FD = c(SN_0')\rho_{snow}d_0/\Delta t \qquad (17)$$

$$\delta^{15}N(FD) = \delta^{15}N(SN_0') \qquad (18)$$

$$\Delta^{17}O(FD) = \Delta^{17}O(SN_0') \qquad (19)$$

The calculated FP and FD in each time step are further used to calculate F_{pri} according to Eq (4-6).

2.3 The choice of model initial conditions

To run the model, an appropriate archival snow nitrate profile with known concentration and isotopic composition ($\delta^{15}N$ and $\Delta^{17}O$) should be assigned as model initial conditions with seasonal or monthly resolution, though ideally weekly or finer resolution data are the best. The archived nitrate profile could be dated by using various types of seasonal markers, such as the $\delta^{18}O$ of H_2O, the ion concentrations or their ratios, and the snow accumulation rates (Hastings et al., 2004; Furukawa et al., 2017; Dibb et al., 2007). As long as the archived snow nitrate profiles (i.e., snow nitrate concentration and isotopes below the photic zone) are given, the model can calculate nitrate concentrations and isotopes throughout the photic zone, and those in the atmosphere. The latter is considered as the atmospheric signals before being affected by post-

depositional processing.

3. Model evaluations

Because ~~there~~ we lack direct observations of primary nitrate, we evaluated the model performance with other kinds of observations, including nitrate isotopes in surface snow and the overlying atmosphere. The deposited nitrate flux FD represents the state of nitrate that has just deposited onto the surface snow via dry deposition of gaseous nitrate or wet scavenge from the atmosphere and is close to the definition of the skin layer of snowpack, i.e., the uppermost several millimeters of surface snow (Erbland et al., 2013; Winton et al., 2020). Thus, if there are sufficient high-resolution skin layer observations, a direct comparison with the model output can be performed (i.e., FD vs. skin layer measurements). Moreover, since FD originates from the local atmosphere, if the air-snow nitrate transfer function (i.e., the mass and isotope relationships between atmospheric nitrate and the deposited nitrate) is known, the calculated FD could be used to infer the state of local atmospheric nitrate. In this study, the isotope transfer function is applied instead of the mass transfer function because of its simplicity, especially for $\Delta^{17}O$, which is assumed to be conserved during deposition owing to its mass-independent nature. For $\delta^{15}N$, we assume that the deposition of atmospheric nitrate is associated with a fractionation constant (ε_d) of +10 ‰ following Erbland et al. (2013). ~~In all, w~~We can either directly compare the modeled isotopes of FD with the observed values in the skin layer or with local atmospheric signals by including the differences (only for $\delta^{15}N$) between FD and atmospheric nitrate.

In this study, we chose two typical polar sites, Summit, Greenland, and Dome C, Antarctica to conduct case studies in order to test the performance of the inverse model. These two sites were chosen for several reasons. First, these two sites represent typical polar sites with both relatively high (Summit) and extremely low (Dome C) snow accumulation rates. Second, there are sufficient atmospheric and/or snow observations at these two sites, which informs model input parameters and allows for comparison of the model results with observations. Third, these two sites are hot spots of ice core drilling, and future work using the inverse model on ice core nitrate records from these

sites can be performed. In addition, there have already been studies simulating the post-depositional processing of snow nitrate at these two sites by using the forward TRANSITS model (Erbland et al., 2015; Jiang et al., 2021). Most of the model parameters in this study are kept the same as the original TRANSITS simulation unless otherwise mentioned. The major parameters used in this study are summarized in Table 2. Below, we specifically describe how we chose the initial model values/conditions for simulations at these two sites.

Table 2. Values of major parameter used in the model simulations at two different sites.

Parameter	Dome C, Antarctica		Summit, Greenland	
	Value	Reference	Value	Reference
FA	1.3×10^{-7} kgN m^{-2} a^{-1}	Erbalnd et al. (2013)	6.7×10^{-6} kgN m^{-2} a^{-1}	Jiang et al., (2022)
$\delta^{15}N(FA)$	273.6 ‰	Erbalnd et al. (2013)	0.6 ‰	Jiang et al., (2022)
$\Delta^{17}O(FA)$	26.0 ‰	Erbalnd et al. (2013)	27.9 ‰	Jiang et al., (2022)
A	28 kg m^{-2} a^{-1}	Erbland et al. (2013)	250 kg m^{-2} a^{-1}	Dibb et al., (2014)
ρ	300	Erbland et al. (2013)	380	Geng et al. (2014)
TCO	175-300 DU	Erbland et al. (2015)	228-494 DU	Jiang et al., (2021)
Φ	0.015	Adjusted[a]	0.002	Jiang et al., (2021)
σ	Wavelength dependent	Berhanu et al. (2014)	Wavelength dependent	Berhanu et al. (2014)
ε_d	+10 ‰	Erbland et al. (2013)	+10 ‰	Erbland et al. (2013)
$\Delta^{17}O(NO_3^-)$ of FP	Observed atmospheric $\Delta^{17}O(NO_3^-)$	Erbland et al. (2013)	Calculated	Jiang et al., (2021)
f_c	0.15	Erbland et al. (2015)	0.15	Erbland et al. (2015)
f_{exp}	0.2	Erbland et al. (2015)	0.35	Jiang et al., (2021)

[a]Adjusted according to the best fit of snowpack nitrate $\delta^{15}N$ profile at Dome C (Appendix C).

	Value	Reference	Value	Reference
A	28 kg m^{-2} a^{-1}	Erbland et al. (2015)	250 kg m^{-2} a^{-1}	Dibb et al., (2014)
Φ	0.015	Adjusted[a]	0.002	Jiang et al., (2021)
f_e	0.15	Erbland et al. (2015)	0.15	Erbland et al. (2015)
f_{exp}	0.2	Erbland et al. (2015)	0.35	Jiang et al., (2021)
ε_d	±10 ‰	Erbland et al. (2013)	±10 ‰	Erbland et al. (2013)
$\Delta^{17}O(NO_3^-)$ of FP	Calculated	Erbland et al. (2013)	Observed atmospheric $\Delta^{17}O(NO_3^-)$	Jiang et al., (2021)

[a]Adjusted according to the best fit of snowpack nitrate $\delta^{15}N$ profile at Dome C (Appendix C).

3.1 Summit, Greenland

Summit, Greenland is a typical site with high snow accumulation rate (250 kg m^{-2} a^{-1}, Dibb et al., 2004) at present, and weekly resolved snow accumulation data exists (Burkhart et al., 2004), allowing for the precise dating of the snowpack nitrate profile (Jiang et al., 2022). The snowpack nitrate concentration and isotope data with weekly resolution at Summit compiled in Jiang et al. (2022) were used as initial model input values to represent the archived snow nitrate signals. The weekly archival snowpack nitrate records at Summit compiled in Jiang et al. (2022) were adapted as initial model values.

3.2 Dome C, Antarctica

The present snow accumulation rate at Dome C, Antarctica is extremely low (28 kg m^{-2} a^{-1}, Erbland et al., 2013), and it is currently impossible to discern seasonal or sub-seasonal nitrate patterns owing to the limited resolution of snowpack measurements. Erbland et al. (2013) reported five snowpack nitrate depth profiles at Dome C that extended just below the photic zone. To predict the final archived nitrate concentration and isotopes, Erbland et al. (2013) fitted these depth profiles with an exponential function, and the obtained asymptotic values were regarded as the final preserved nitrate signal. The average asymptotic values for the five snowpacks were (21.2 ± 18.1)

ng g^{-1}, (273.6 ± 64.0) ‰ and (26.0 ± 1.9) ‰ for nitrate concentration, δ^{15}N and Δ^{17}O, respectively. These values were used as the annual averages of the preserved nitrate at Dome C in this study.

370 We note the seasonality of the archived nitrate concentration is important because it determines the magnitude of FP and FD at each time step in the model. In simulations of Dome C, we designed three cases with different weekly concentration distributions in a year. In case 1, the weekly nitrate concentrations were assumed to be uniform throughout a year. In case 2, the weekly archival nitrate concentrations were assumed to be a Gaussian-type distribution to match the observed seasonality in skin layer nitrate

375 concentrations at Dome C (Erbland et al., 2013):

$$c(n) = c_a \times \left(a + b \times \exp\left(-\frac{(n - n_0)^2}{\sigma^2} \right) \right) \qquad (20)$$

In Eq (20), c_a represents the annual average snow nitrate concentration, n represents the week number (1 to 52, here week 1 is defined as the first week in January for the northern hemisphere sites or the first week in July for the southern hemisphere sites)

380 and the shape parameters (a, b, σ) were determined by the best fit of skin layer nitrate concentrations (Appendix D). n_0 represents the week when nitrate concentration peaks in a year and was set to be 26 according to the observed maximum nitrate concentrations in the skin layer in local midsummer (Erbland et al., 2013). However, since nitrate deposited in different weeks of a year would have experienced different amounts of

385 total actinic flux and nitrate deposited in autumn undergoes minimal degree of photolysis (Jiang et al., 2022), it is likely that the summer peak would shift toward autumn by final preservation. As such, we also prescribed a "shifted peak" distribution in case 3, and in this case n_0 was set equal to 35 in Eq. (20), while other parameters were the same as in case 2.

390 To determine the uncertainties in the model results caused by these artificially assumed nitrate profiles, we applied a Monte Carlo method, i.e., the exact initial value in snow at each week was set arbitrarily as follows:

$$c_r = c_a + \mathbf{U}(-\sigma, \sigma) \qquad (21)$$

where c_a represents the prescribed initial value of annual-mean snow nitrate concentration in each case as described above, **U** represents a uniformly distributed random variable and σ represents the standard error of the observed c_a. The obtained time series with random error was normalized again as final model inputs. All three cases were repeated 1000 times, and the model results were used to evaluate the uncertainties.

For isotopic ratios ($\delta^{15}N$ and $\Delta^{17}O$) of the archived nitrate, their seasonality was omitted in this study to simplify the model calculations, and for the results at Dome C we only compared the modeled results with observations at annual scale given the unknown seasonal inputs of these parameters. Note that reconstruction of atmospheric signals of $\delta^{15}N$ and $\Delta^{17}O$ from ice core records usually use a coarser resolution than sub-annual variations, justifying our annual averaging approach.

4. Results and discussion

4.1 Model results at Summit, Greenland

4.1.1 Comparison of local atmospheric variations
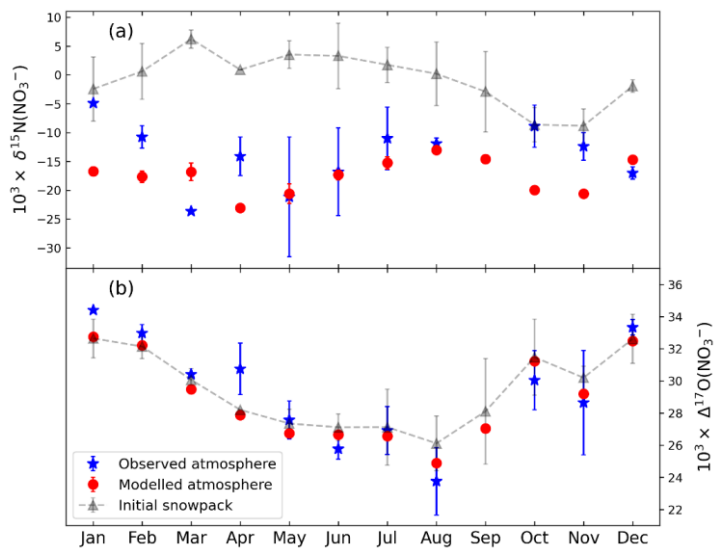
Figure 3. Comparison between the modeled (red dots) and observed (blue stars) seasonal variations in atmospheric nitrate (**a**) $\delta^{15}N$ and (**b**) $\Delta^{17}O$ at Summit Greenland. The dashed line with gray triangle represents the snowpack measurements as model

inputs (i.e., the monthly archived snow nitrate $\delta^{15}N$ and $\Delta^{17}O$ from snowpack observations) (Jiang et al. 2022). The atmospheric observations were from Jiang et al.

415 (2022).

Currently there are no skin layer observations at Summit, so we used the monthly atmospheric nitrate isotopic data from aerosol observations at Summit reported by Jiang et al. (2022) to compare with the modeled atmospheric nitrate isotopic variations and the atmospheric nitrate isotopes reported by Jiang et al. (2022) were used for model

420 comparison. To reduce the uncertainty of model results owing to uncertainties associated with the weekly dating of snowpack, we only compared the modeled monthly averages with observations, and the uncertainties of the monthly model results were calculated as one standard error of the mean of results from different weeks. As shown in Fig. 3, the modeled seasonality in atmospheric $\Delta^{17}O(NO_3^-)$ generally agrees

425 well with the observed seasonal variations, while for $\delta^{15}N(NO_3^-)$, the model predicted a similar seasonality as the observations, though in the winter half year the model underestimated the absolute values in comparison with the observations As shown in Fig. 3, the modeled seasonal variations in atmospheric $\delta^{15}N(NO_3^-)$ and $\Delta^{17}O(NO_3^-)$ agree well with the observed seasonality. In addition, the modeled and observed

430 atmospheric $\Delta^{17}O(NO_3^-)$ are both close to snowpack $\Delta^{17}O(NO_3^-)$. This is just as expected at Summit since the deposition of atmospheric nitrate is assumed to be a mass-dependent process. The only process that can alter $\Delta^{17}O(NO_3^-)$ in snow is the cage effect (McCabe et al., 2005), which is negligible under present Summit conditions. The inverse model calculated a small cage effect of 0.15 ‰ on $\Delta^{17}O(NO_3^-)$ by comparing

435 the annual weighted average of FA and FD, which is close to the value of 0.19 ‰ predicted by the TRANSITS model (Jiang et al., 2021). At an annual scale, the modeled and observed average atmospheric $\delta^{15}N(NO_3^-)$ are -17.5 ± 3.0 ‰ and -14.8 ± 7.3 ‰, while for $\Delta^{17}O(NO_3^-)$ the values are 28.8 ± 2.6 ‰ and 28.6 ± 3.2 ‰ respectively, suggesting that the inverse model reproduced the atmospheric observations quite well.

440 For $\delta^{15}N(NO_3^-)$, the modeled atmospheric $\delta^{15}N(NO_3^-)$ seasonality is comparable to the observations, but the absolute values display some discrepancies in autumn and winter. In particular, the modeled and observed average $\delta^{15}N(NO_3^-)$ values in the

summer half-year (from March to August) are -17.6 ± 3.5 ‰ and -16.0 ± 7.8 ‰, respectively, while in the winter half-year they are -16.0 ± 7.8 ‰ and -12.0 ± 4.1 ‰,

445 respectively. The model-observation difference in the winter half year may be related to the model set-up of a constant ε_d of +10 ‰. As discussed by Jiang et al. (2022), the partition between nitrate deposition mechanisms (i.e., wet vs. dry deposition) may result in seasonally different air-snow transfer functions for $\delta^{15}N(NO_3^-)$. It has been observed that $\delta^{15}N(NO_3^-)$ of dry deposition is generally higher than wet deposition (Beyn et al.,

450 2014; Heaton, 1987). This implies that dry deposition likely possesses a larger ε_d, perhaps because wet deposition can scavenge all or most of atmospheric nitrate, leading to small to no isotope fractionation. Given the potential seasonal changes in the relative fraction of dry versus wet deposition at Summit, using a constant ε_d in the model would likely cause discrepancies in one season but not in the other. Some observations at

455 Summit indicate that snowfall activities are more frequent and severe in summer months (June-September) than in winter (Castellani et al., 2015; Bennartz et al., 2019), which implies that dry deposition of atmospheric nitrate is more important in winter instead of summer. Thus, the model-observation discrepancies in the winter half year cannot be explained by the seasonal shift in the ratio between wet and dry deposition,

460 as more dry deposition may result in a larger isotope effect in winter.

Alternatively, we note the ε_d itself may have a seasonality which could be caused by the temperature dependence of nitrate absorption onto ice grains (Abbatt, 1997) or be influenced by other mechanisms such as the stability of the boundary layer. In fact, observations at Dome C indicated the averaged enrichment in skin layer $\delta^{15}N(NO_3^-)$

465 related to atmospheric $\delta^{15}N(NO_3^-)$ is +25 ‰ in summer, while in winter the value is +10 ‰ (Erbland et al., 2013). This may indicate a larger ε_d in summer than in winter, though the summer skin layer $\delta^{15}N(NO_3^-)$ is probably more or less influenced by photolysis which tends to increase $\delta^{15}N(NO_3^-)$. However, in the inverse model, ε_d was set as +10 ‰ throughout the year for Summit (note this value is consistent with the

470 observed difference between surface snow and local atmospheric $\delta^{15}N(NO_3^-)$ at Summit in May and June (Fibiger et al., 2016)). If at Summit the ε_d in winter is lower than that

in summer, the modeled average $\delta^{15}N(NO_3^-)$ in the winter half year would have been underestimated. This at least explains in part the model-observation discrepancies in winter half year $\delta^{15}N(NO_3^-)$. Future work on the degree of nitrogen isotope fractionation during atmospheric nitrate deposition and the causal factors are necessary to further investigate this issue.

4.1.2 Flux and isotopes of primary nitrate
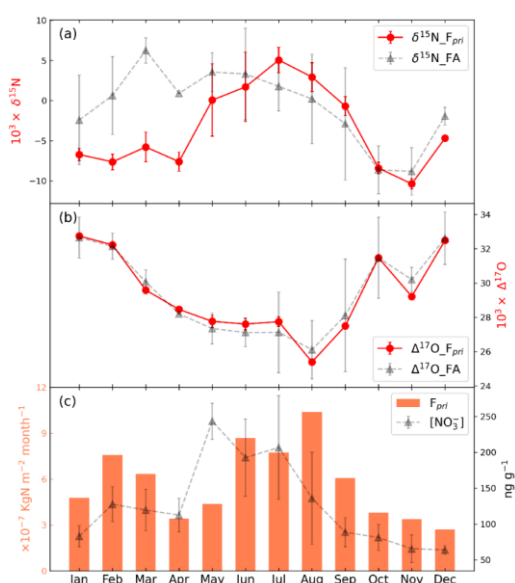
Figure 4. The modeled monthly (**a**) $\delta^{15}N$, (**b**) $\Delta^{17}O$ and (**c**) fluxes of primary nitrate (F_{pri}) to Summit Greenland. The concentration, $\delta^{15}N$ and $\Delta^{17}O$ values of the archived snow nitrate as model inputs are also shown for comparison (gray triangle with dashed line).

The major function of the inverse model is to reconstruct the primary nitrate flux and its isotopes by using ice core nitrate records. Primary nitrate flux is closely associated with atmospheric nitrate on the regional scale and could be further linked to the atmospheric abundance of its precursor NO_x. The isotopic composition of F_{pri} could provide extra information. For example, the $\delta^{15}N$ of F_{pri} may be used to infer the variations in NO_x source emissions if other factors influencing isotope fractionation during the atmospheric conversion of NO_x to nitrate can be constrained. The $\Delta^{17}O$ of

F_{pri} depends on the relative concentration of major atmospheric oxidations such as O_3 and HO_2/RO_2 radicals and thus could be used to reflect regional atmospheric oxidation environment (Geng et al., 2017; Sofen et al., 2014).

The model-calculated seasonal variations in F_{pri} to Summit are shown in Fig. 4. The annual flux of primary nitrate was calculated to be 6.96×10^{-6} kgN $m^2 a^{-1}$, which is ~~similar~~ in the same range ($\approx$ 2-3 $\times 10^{-6}$ kgN $m^2 a^{-1}$) ~~to~~ as model results from Zatko et al. (2016) using the GEOS-Chem model and is about two orders of magnitude lower than the atmospheric nitrate deposition flux in mid-latitude area (Gao et al., 2019; Zhang et al., 2012). The seasonality of F_{pri} displays a bimodal mode with a major summer peak and a secondary peak in late winter/early spring, in contrast the preserved snowpack nitrate concentration which peaks in spring/summer. The maximum F_{pri} in summer could be caused by the enhanced temperature-dependent precursor NO_x emissions such as from soil microbes (Pilegaard et al., 2006) as well as the more active photochemistry in summer, both of which would promote more efficient atmospheric nitrate production. It is interesting that the secondary F_{pri} peak in early spring is coincident with the timing of the spring Arctic haze phenomenon (Quinn et al., 2007), as well as the occasional spring nitrate concentration peak in snowpack and ice cores at Summit (Geng et al., 2014), though the exact timing of the seasonal peaks needs further investigation.

The modeled $\Delta^{17}O$ of F_{pri} is close to the measurements in the snowpack with minimum values in summer, suggesting the $\Delta^{17}O$ signal of primary nitrate is well preserved under current Summit conditions. The seasonal variations in $\Delta^{17}O$ of F_{pri} can be understood in terms of the different production mechanisms of atmospheric nitrate (Alexander et al., 2020). In summer, ample solar radiation enhances the photochemical production of HNO_3 from the NO_2+OH pathway, the $\Delta^{17}O$ of which is lowest compared with other nitrate formation pathways. While in winter, the dominant N_2O_5 hydrolysis pathway produces nitrate with high $\Delta^{17}O$. Such seasonal patterns have been widely observed globally as summarized in Alexander et al. (2020).

The modeled $\delta^{15}N$ of F_{pri} ranges from -10.3 ‰ to 5.0 ‰ which falls well within

the reported atmospheric $\delta^{15}N(NO_3^-)$ values in continental and marine boundary layer in both hemispheres in regions not impacted by snowpack emission (Li et al., 2022; Lim et al., 2022; Morin et al., 2009; Shi et al., 2021). However, the seasonal pattern of $\delta^{15}N$ of F_{pri} which displays a summer maximum is opposite to the typical seasonal pattern of atmospheric $\delta^{15}N(NO_3^-)$ found in mid-latitude continental areas, where higher $\delta^{15}N(NO_3^-)$ values in winter and lower $\delta^{15}N(NO_3^-)$ values in summer are widely observed (e.g., Beyn et al., 2014; Freyer, 1991; Fang et al., 2021; Lim et al., 2022; Esquivel Hernández et al., 2022). This summer high and winter low $\delta^{15}N(NO_3^-)$ in F_{pri} is instead consistent with the observations at two Arctic coastal sites (Morin et al., 2012; Morin et al., 2008), where the summer high atmospheric $\delta^{15}N(NO_3^-)$ is strongly correlated with air temperature. Morin et al. (2008) suggest the $\delta^{15}N(NO_3^-)$-temperature relationship observed at the Arctic coastal sites may be related to physicochemical transformations of nitrate in the Arctic and during the transport of nitrate and reactive nitrogens from the mid-latitudes, though the specific mechnisms~~mimes~~ is unknoonwn.

Another possibility to explain the higher modeled summer ~~higher~~ $\delta^{15}N(NO_3^-)$ in F_{pri} is that there may be more anthropogenic nitrate transported from mid-latitudes to Greenland in summer than in winter. F_{pri} is comprised of nitrate originating from the mid-latitudes as well as nitrate formed in the Arctic region. Morin et al. (2009) suggested that air parcels originating from regions with more anthropogenic impacts carries nitrate with higher $\delta^{15}N$, which was confirmed by subsequent studies (Li et al., 2022; Vicars and Savarino, 2014; Shi et al., 2021). The increased frequency of air sources originating from the North America in summer compared to winter (Kahl et al., 1997) could thus lead to more anthropogenic nitrate to Greenland in summer, resulting in higher summer $\delta^{15}N$ of primary nitrate than winter.

The potential link between $\delta^{15}N$ of F_{pri} and its precursor NO_x emissions is not further discussed here, as recent studies have shown that the isotopic effect during NO_x photo-recycling is complex (Li et al., 2020) and may dominate $\delta^{15}N$ variations in atmospheric nitrate (Fang et al., 2021; Li et al., 2021). More comprehensive studies on the isotopic effects during atmospheric nitrate formation as well as the potential

fractionation during transport are required to further link δ^{15}N of F$_{pri}$ with its precursors
and/or source regions.

4.2 Model results at Dome C, Antarctica

4.2.1 Snowpack nitrate profile in the photic zone
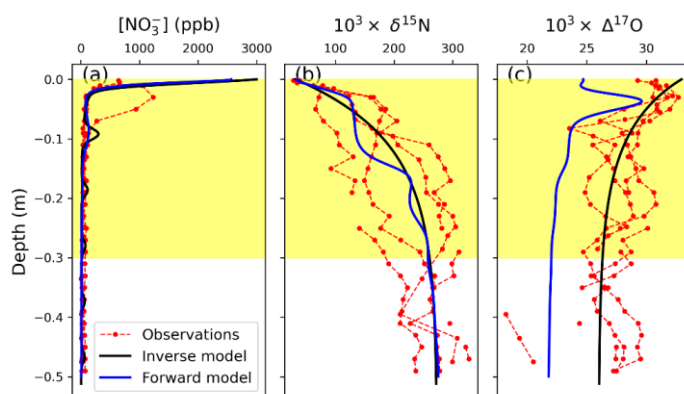
Figure 5. Comparison between the observed and modeled snowpack nitrate
concentrations, δ^{15}N, and Δ^{17}O at Dome C. The red lines with circles represent four
observed snowpack nitrate profiles at Dome C from Erbland et al. (2013) and Frey et
al. (2009), while the blue and black lines are modeled results from the forward model
(i.e., the TRANSITS model) and the inverse model in this study, respectively. The
yellow background represents the depth of the photic zone.

Since Dome C snowpack exhibits very distinct trends in the concentration and
isotopic ratio of nitrate in the photic zone, we first examine the modeled summer
snowpack nitrate profile at Dome C in comparison with the previous observations
(Erbland et al., 2013; Frey et al., 2009) in Fig. 5. The TRANSITS model results
(Erbland et al., 2015) are also shown in Fig. 5 for comparison. Both models reproduce
the observed decrease in nitrate concentration and the large enrichments in δ^{15}N(NO$_3^-$)
well. We note that the predicted surface snow nitrate concentration is higher than the
observations by both models. This is because the modeled concentration represents the
state that atmospheric nitrate has just deposited onto the snow surface, while the
observed skin layer snow may have already undergone snow metamorphism and/or
post-depositional processing (Winton et al., 2020). This is also supported by recent

observations at Dome C that newly deposited diamond dust could possess nitrate concentrations up to 2000 ppb (Winton et al., 2020), within the range of model predictions.

575   The decreasing trend in $\Delta^{17}O(NO_3^-)$ within the photic zone is also reproduced by these two models, caused by the cage effect during nitrate photolysis. However, the TRANSITS model appears to underestimate snowpack $\Delta^{17}O(NO_3^-)$ while the inverse model performs better in snowpack $\Delta^{17}O(NO_3^-)$ simulation. This is because in the TRANSITS model, snow $\Delta^{17}O(NO_3^-)$ is controlled by a combination of $\Delta^{17}O(NO_3^-)$ of

580   FD and the subsequent cage effect after deposition. At Dome C, $\Delta^{17}O(NO_3^-)$ of FD is dominated by locally formed atmospheric nitrate (i.e., FP) (Erbland et al., 2015), which is in turn determined by the prescribed $\Delta^{17}O$ transfer during NO-NO$_2$ cycling and the subsequent OH oxidation of NO$_2$ under sunlight conditions in the model. However, Savarino et al. (2016) demonstrated that the standard chemistry (i.e., exclusive

585   oxidation of NO$_2$ by OH in summer) and the associated isotopic mass balance applied to $\Delta^{17}O$ (i.e., the one used by the direct model) does not hold in the Dome C atmosphere, with this standard approach systematically underestimating the observations. Our inverse model is in line with this conclusion. The inverse model calculates atmospheric $\Delta^{17}O(NO_3^-)$ from the archived snow $\Delta^{17}O(NO_3^-)$ by subtracting the cage effect but does

590   not assume any specific chemical reaction in the atmospheric box, contrary to the forward model. Therefore, although the inverse model uses the same method as the TRANSITS model to calculate $\Delta^{17}O(NO_3^-)$ of locally formed atmospheric nitrate (FP), it does not include any hypothesis of how local nitrate is formed. The good match between observations and inverse model output is a further demonstration that

595   atmospheric $\Delta^{17}O(NO_3^-)$ is not in agreement with the standard daylight chemistry of nitrate formation (i.e. NO$_2$+OH).

        Overall, the consistency of the modeled and observed snowpack nitrate profiles suggests that the effect of post-depositional processing is properly represented by the inverse model. This confirms that the inverse model can properly reproduce snow

600   nitrate concentrations and isotopes in the photic zone, which are intermediate statuses

between archived and atmospheric nitrate.

4.2.2 Skin layer and atmospheric nitrate
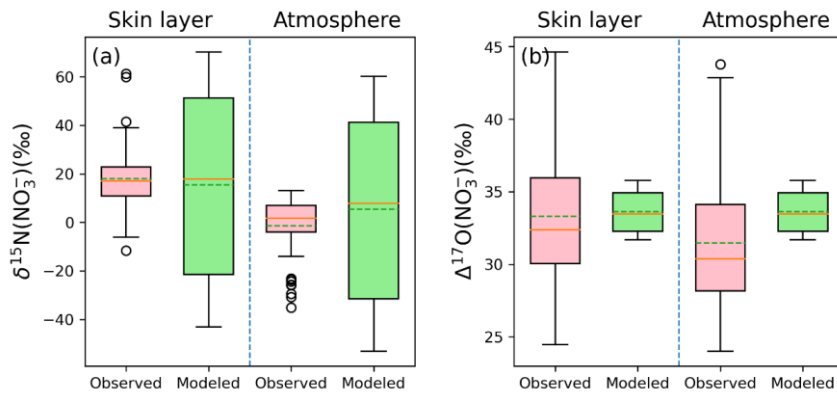
Figure 6. Comparison between the observed and modeled annual averages of $\delta^{15}N(NO_3^-)$ and $\Delta^{17}O(NO_3^-)$ in the atmosphere and snow skin layer at Dome C. The solid line in the box plot indicates the median value, while the dash line represents the average value.

~~For Dome C, since the seasonal information of the archived nitrate profiles is unknown, A~~althougha~~a~~lthough the time step in the model was set to one week for Dome C, we mainly focus on the annual average values since the seasonal information of the archived nitrate profiles is unknown. We note that the modeled isotopic compositions of snowpack and skin layer nitrate are not affected by~~irrelevant to~~ the prescribed nitrate concentration seasonality. This is because the total nitrate loss fraction and the induced isotopic effect only depend on the total amount of actinic flux received during snow burial. In the following discussion we only report and discuss the modeled isotopes of local atmospheric and skin layer nitrate from case 1, i.e., the archived snow nitrate concentration was assumed to be constant throughout the year.

The observed annual average $\delta^{15}N(NO_3^-)$ and $\Delta^{17}O(NO_3^-)$ values in the skin layer at Dome C are 18.0 ± 11.7 ‰ and 33.6 ± 1.4 ‰, respectively (Erbland et al., 2013), while the modeled skin-layer values are 15.7 ± 38.6 ‰ and 33.3 ± 4.7 ‰, respectively, in good agreement with the observations. The observed annual average atmospheric $\delta^{15}N(NO_3^-)$ and $\Delta^{17}O(NO_3^-)$ values are -1.3 ± 11.6 ‰ and 31.4 ± 4.6 ‰, respectively, while the modeled values are 8.0 ± 11.7 ‰ and 33.6 ± 1.4 ‰, respectively. Note the

average observed δ^{15}N values in this study were calculated as arithmetic mean instead

of mass-weighted mean reported in Erbland et al. (2013) since the inverse model cannot

directly calculate the nitrate concentration in the atmosphere. Nevertheless, the

modeled averages are similar to the observed averages except for atmospheric

δ^{15}N(NO$_3^-$). The difference between the modeled and observed atmospheric δ^{15}N(NO$_3^-$)

could be again related to the constant ε_d used in the model. As discussed earlier, in the

model we followed Erbland et al. (2015) to set $\varepsilon_d = 10$ ‰ throughout the year, while

observations at Dome C indicate that ε_d could be as large as 25 ‰ in summer instead of

10 ‰ (Erbland et al., 2013). Hence the modeled atmospheric δ^{15}N(NO$_3^-$) could be

overestimated. This reinforces that it is necessary to further explore the isotope effects

on δ^{15}N(NO$_3^-$) during atmospheric nitrate deposition.

4.2.3 Flux and isotopes of primary nitrate
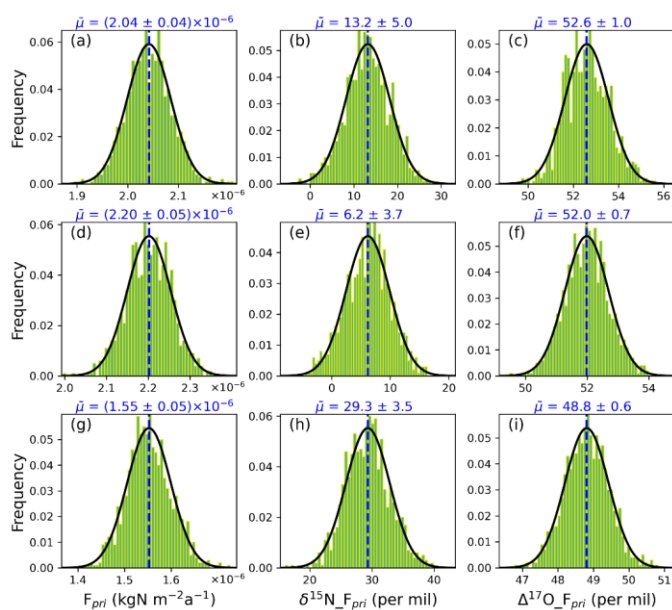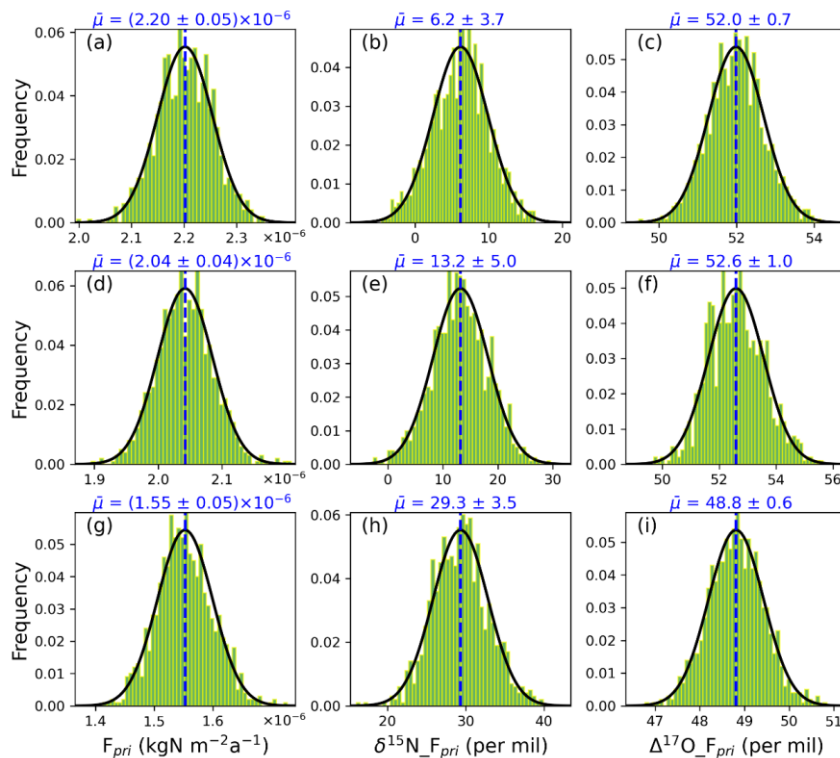
Figure 7. Frequency histogram of the calculated primary nitrate flux and its mean $\delta^{15}N/\Delta^{17}O$ values at Dome C under three different archival snow nitrate concentration distributions: (**a-c**) Case 1: uniform distribution, (**d-f**) Case 2: Gaussian-type function, (**g-i**) Case 3: shifted Gaussian-type function. The black solid lines represent the fitted Gaussian function of the frequency distribution. The blue dashed lines represent the mean values of F_{pri} and its $\delta^{15}N$ and $\Delta^{17}O$, which are labeled on the top of each subplot.

In Fig. 7, the flux of primary nitrate (F_{pri}) and its mean isotopes from the 3 difference cases (i.e., different nitrate concentration seasonality in archived snow) are displayed. Similar to the previous section, we only focus on their annual means. Note when calculating $\Delta^{17}O(NO_3^-)$ of F_{pri}, $\Delta^{17}O$ values of locally formed nitrate are necessary. As discussed in 4.2.1, ~~that~~ following the ~~same~~ method in the TRANSITS model to calculate $\Delta^{17}O(NO_3^-)$ of locally formed atmospheric nitrate would underestimate $\Delta^{17}O(NO_3^-)$ of FP at Dome C. This is especially evident in summer when the snow sourced nitrate (i.e., FP) dominates the atmospheric nitrate budget, and the calculated

批注 [zj1]: In previous Fig. 7 we mistook the order of model results in case 1 and case 2 and this error has been corrected in the revised version. This point doesn't influence the conclusions.

$\Delta^{17}O(NO_3^-)$ of FP by the TRANSITS model is about 6 ‰ lower than observed atmospheric $\Delta^{17}O(NO_3^-)$ (Erbland et al., 2015). Thus, in the inverse model, when calculating $\Delta^{17}O(NO_3^-)$ of F_{pri} at Dome C, $\Delta^{17}O(NO_3^-)$ of FP was not calculated using the model default method as in the TRANSITS, but prescribed as the observed atmospheric summer $\Delta^{17}O(NO_3^-)$. Otherwise, the modeled $\Delta^{17}O(NO_3^-)$ of F_{pri} would be higher than 70 ‰, which is highly unrealistic. Note, this is not an issue at Summit Greenland because FP doesn't dominate the atmospheric nitrate budget in summer there.

As shown in Fig. 7, although the prescribed archived nitrate concentration seasonality does not alter the modeled snowpack and atmospheric nitrate isotopes, it has a profound impact on the modeled primary nitrate flux and its isotopes. In particular, under the three cases of different seasonal distributions of the archived snow nitrate concentrations, the modeled F_{pri} and its annual mean $\delta^{15}N$ and $\Delta^{17}O$ range from 1.5 to 2.2 $\times 10^{-6}$ kgN m^{-2} a^{-1}, 6.2 to 29.3 ‰ and 48.8 to 52.6 ‰, respectively. The inverse model calculated F_{pri} is smaller than the value used in the original TRANSITS (8.2×10^{-6} kgN m^{-2} a^{-1}) in Erbland et al. (2015), but this is easily resolved given the large uncertainty in the archived nitrate concentration used as model input.

The modeled annual mean $\delta^{15}N$ of F_{pri} ranges from 6.2-29.3 ‰, in contrast with the observed atmospheric $\delta^{15}N(NO_3^-)$ in southern mid-latitude area or the Southern Ocean where $\delta^{15}N(NO_3^-)$ is in general negative or close to 0 (Morin et al., 2009; Shi et al., 2018; Shi et al., 2021). The modeled positive $\delta^{15}N$ of F_{pri} is however consistent with the wintertime atmospheric $\delta^{15}N(NO_3^-)$ observed in Antarctica when the effect of photolysis is null and local atmospheric nitrate likely reflects F_{pri}. The maximum atmospheric $\delta^{15}N(NO_3^-)$ in winter was found to be 10.8 ‰ at DDU (Savarino et al., 2007), 12.8 ‰ at Dome C (Erbland et al., 2013) and 13.9 ‰ at Zhongshan station (Shi et al., 2022). These positive $\delta^{15}N$ values have been link to stratospheric denitrification as nitrate produced in stratosphere is suggested to be 19 ± 3 ‰ by considering the fractionation induced by different of N_2O photolysis channels (Savarino et al., 2007). Therefore, the modeled flux and $\delta^{15}N$ of F_{pri} points towards the dominance of stratospheric denitrification in nitrate budget at Dome C.

The modeled $\Delta^{17}O$ of F_{pri} is also very high for all three cases (48.8-52.6 ‰). The measured bulk $\Delta^{17}O$ of surface ozone in Antarctica is about 26 ‰ (Ishino et al., 2017; Savarino et al., 2015) that fits well with the global tropospheric average of 25.4 ‰ (Vicars and Savarino, 2014). Given that the oxygen mass-independent fractionation signal of ozone is mainly occupied by the terminal oxygen atom and transferred to other molecular, atmospheric nitrate of tropospheric origin should possess a $\Delta^{17}O$ signal less than 39 ‰ (Mauersberger et al., 2003; Savarino et al., 2008), which cannot explain our calculated high $\Delta^{17}O$ of F_{pri}. However, the bulk $\Delta^{17}O$ of stratospheric ozone was measured to be 34.3 ± 3.6 ‰ (Lämmerzahl et al., 2002; Krankowsky et al., 2000), which indicated that nitrate produced in the stratosphere could gain a higher $\Delta^{17}O$ signature from ozone (Lyons, 2001). It has been observed in Antarctica that the atmospheric $\Delta^{17}O(NO_3^-)$ could exceed 40 ‰ in winter and early spring when stratospheric denitrification occurs (Ishino et al., 2017; Walters et al., 2019; Erbland et al., 2013; Savarino et al., 2007; Shi et al., 2022). A recent study also revealed that the surface snow $\Delta^{17}O(NO_3^-)$ at Dome C frequently exceeds 40 ‰ during winter/spring and could sometimes reach up to 50 ‰ (Akers et al., 2022). As we mentioned previously, these winter $\Delta^{17}O(NO_3^-)$ observations likely reflect the primary nitrate signal at that time since the photolysis of snow nitrate does not occur due to lack of sunlight. Thus, the high modeled $\Delta^{17}O$ of F_{pri} seems to again indicate a dominant role of stratosphere denitrification in external nitrate source to Dome C, similar to what can be reflected from the modeled $\delta^{15}N$ of primary nitrate. In addition, Erbland et al (2015) estimated that stratospheric denitrification nitrate flux is $(4.1 \pm 2.5) \times 10^{-6}$ kgN m^{-2} a^{-1} in Antarctica, while our calculated F_{pri} of $1.5 - 2.2 \times 10^{-6}$ kgN m^{-2} a^{-1} at Dome C is within the same range.

In sum, we acknowledge that there are many factors that would affect the model results, such as the archived snow nitrate concentration and isotopes, the export fraction (f_{exp}), and the cage effect fraction (f_c). These need to be further explored by observations to improve the model performance.

5. Model sensitivity tests: the impact of f_{exp} and f_c

In this section, we report the sensitivity test results to elucidate the impact of two model parameters that lack ~~of~~ direct observational constraints, the export fraction (f_{exp}) and the cage effect fraction (f_c). We mainly focus on the annual net loss and the differences in isotopes between F_{pri} and FA in accordance with the resolution of ice core measurements.
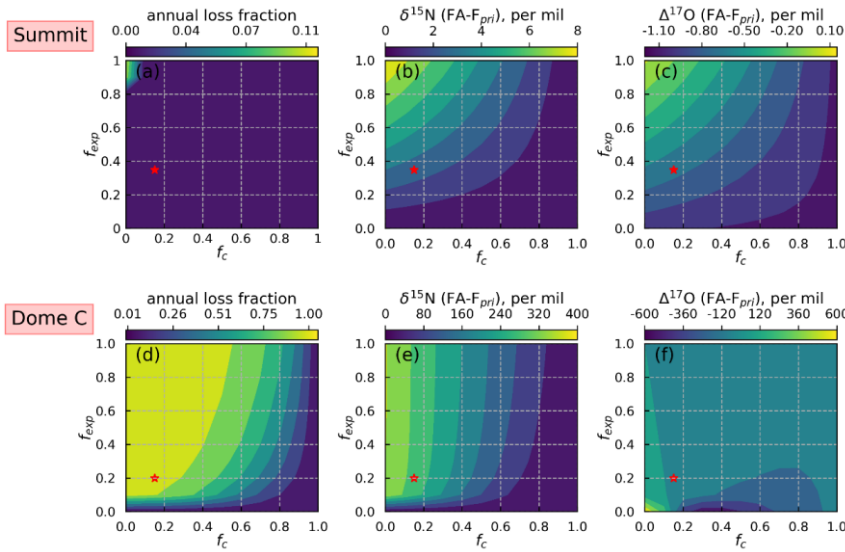
Figure 8. Model sensitivity test results of two parameters f_{exp} and f_c for Summit (**a-c**) and Dome C (**d-f**). The annual nitrate loss fraction is defined as $1-FA/F_{pri}$ following Jiang et al. (2021). Red stars represent the values of f_{exp} and f_c used in model simulations.

The sensitivity test results are shown in Fig 8. The annual loss fraction (defined as $1-FA/F_{pri}$) represents the final preservation of primary nitrate after post-depositional processing (Jiang et al., 2021). The inverse model predicts an annual loss fraction of 3.5% under present Summit conditions, which is close to the TRANSITS model prediction of 4.1% (Jiang et al., 2021). This small discrepancy is likely caused by the use of simplified snow radiative transfer parameterization in the inverse model. In addition, the differences of $\delta^{15}N$ and $\Delta^{17}O$ between FA and F_{pri} are also in good agreement with the TRANSITS model. As expected, larger f_{exp} and smaller f_c would result in a higher degree of net loss in F_{pri} and larger isotopic effects in both $\delta^{15}N$ and $\Delta^{17}O$. However, under present-day conditions at Summit, the preserved snow nitrate

concentrations and isotopes at the annual scale is only altered slightly and the degree of changes is insensitive to f_{exp} and f_{c}.

For Dome C, the model results are sensitive to f_{exp} when f_{c} is small, and becomes sensitive to f_{c} when f_{exp} is larger. In particular, the isotopic signature is largely independent of f_{exp} when f_{exp} is larger than 0.1-0.2. In addition, the $\Delta^{17}O$ results display a non-monotonic response to these two parameters, especially when f_{exp} approaches zero (Fig. 8f). A similar phenomenon was seen in the TRANSITS model simulations in Erbland et al. (2015), where they found that the model results could not converge when f_{exp} was set to zero. The high sensitivity of model parameters renders difficult to reconstruct the historical variations in primary nitrate based on ice core records at Dome C unless these parameters are precisely constrained. For present day conditions, f_{exp} and f_{c} could be constrained by atmospheric and snowpack observations (Erbland et al., 2015) but it is unknown if these values could be applied to different climate conditions. In addition, the difficulties in choosing an appropriate archival nitrate concentration profile as model initial conditions would add extra uncertainties to the model results.

6. Conclusions and implications

In this study, we introduce an inverse model which is designed to correct for the effects of post-depositional processing on ice-core nitrate concentration and its isotopes. The model was tested against present-day Summit, Greenland and Dome C, Antarctica conditions to validate its performance under different snow accumulation rates. Model results compared to observations demonstrate that the inverse model is capable of adequately correcting the effect of post-depositional processing. The modeled atmospheric nitrate $\delta^{15}N/\Delta^{17}O$ at Summit are generally in good agreement with observations but with slight underestimate in winter $\delta^{15}N(NO_3^-)$, which is likely because the model doesn't treat ~~the~~ correctly the seasonal differences in nitrogen isotope fractionation during deposition (ε_{d}). At Dome C, the model also well reproduced the observed snowpack nitrate profiles in the photic zone, the annual skin layer $\delta^{15}N/\Delta^{17}O(NO_3^-)$, and atmospheric $\Delta^{17}O(NO_3^-)$ at Dome C, but again overestimated the average atmospheric $\delta^{15}N(NO_3^-)$ probably also due a low bias in ε_{d} used in the model.

760   A better quantification on the isotope fractionation of $\delta^{15}N(NO_3^-)$ during deposition is therefore needed.

The inverse working flow of this new model also enables us to qualitatively retrieve information regarding primary nitrate from the archived snow nitrate. The calculated seasonality in $\delta^{15}N$ of F_{pri} at Summit displays a maximum in mid-summer that is distinct

765   from the observed spring $\delta^{15}N(NO_3^-)$ peak in snowpack. This seasonal pattern is in contrast with observed atmospheric $\delta^{15}N(NO_3^-)$ variations in mid-latitudes which is thought to be the major aerosol source region to Summit, but is consistent with the atmospheric $\delta^{15}N(NO_3^-)$ variations observed in the high-latitude Arctic region. The $\delta^{15}N$ of F_{pri} may reflect seasonally-varied main source regions to Greenland or a dominate

770   role of high-latitude nitrate transport to Summit. At Dome C, both the magnitude of F_{pri} and its $\delta^{15}N/\Delta^{17}O$ indicate a dominant role of stratospheric denitrification on nitrate budget at Dome C.

The inverse model is designed to help interpret ice core nitrate records. Applying the inverse model to ice core nitrate records needs knowledge of initial conditions. In

775   particular, archived snow nitrate concentration and its $\delta^{15}N$ and $\Delta^{17}O$, the snow accumulation rate and light absorption impurity concentrations should be known for a given ice core. In addition, chemistry-climate models such as the ICECAP or GCAP model (Murray et al., 2021; Murray et al., 2014) would be also necessary to provide extra constraints, such as the oxidizing agent concentrations, total column ozone (TCO),

780   wind field and boundary layer heights for the past climates and are required to estimate $\Delta^{17}O$ of FP and f_{exp} (Alexander et al., 2020; Jiang et al., 2021). The calculated primary nitrate flux and its $\delta^{15}N$ and $\Delta^{17}O$ can be further combined with the chemistry-climate model results to interpret its climate implications such as the variations in tropospheric NO_x and oxidant abundance, which would improve our understanding of key factors

785   controlling the variability in atmospheric oxidation capacity under different climates.

Appendix A: derivation of the nitrate mass and isotopic balance equations during photolysis (Eq (7-9))

In the inverse model, we follow Erbland et al. (2015) to separate the photolysis

process of nitrate on an ice grain into two steps, i.e., the direct photolysis followed by the subsequent cage effect (Fig. A1). It is well-documented that secondary chemistry can occur during snow nitrate photolysis to reform nitrate and alter the isotopes of the remaining nitrate, which is termed as the cage effect (McCabe et al., 2005; Meusinger et al., 2014). To quantify this effect, Erbland et al. (2015) assigned an empirical parameter (f_c) to represent the fraction of the nitrate photoproducts that would undergo the cage effect, and derived a value of 0.15 for f_c based on the observed decreasing trend of $\Delta^{17}O$ (NO_3^-) in the snowpack at Dome C. As shown in Fig. A1, assuming a fraction (f_p) of initial snow nitrate was photolyzed and a fraction (f_c) of these photolyzed nitrate undergone cage effect, the mass balance equation for snow nitrate can be written as:

$$c(SN) = c\left(SN'\right)\left(1 - f_p + f_c f_p\right) \tag{A1}$$

~~We follow the previous appoint that~~ where the superscript represents the state before photolysis. It can be easily seen that Eq (A1) is equal to Eq (7).

The direct photolysis of snow nitrate can be described by the Rayleigh equation. We define the first-order photolysis rate constant of $^{14}NO_3^-$ and $^{15}NO_3^-$ as J and J^* and their concentration in snow as c and c^* respectively. The chemical kinetic equations of c and c^* can be represented as follows:

$$\frac{dc}{dt} = -Jc \tag{A2}$$

$$\frac{dc^*}{dt} = -J^*c^* \tag{A3}$$

Integrating Eq(A2) and Eq(A3) yields Eq(A4) and Eq(A5):

$$c(t) = c(0)e^{-\int_0^t J dt} \tag{A4}$$

$$c^*(t) = c^*(0)e^{-\int_0^t J^* dt} \tag{A5}$$

Here $c(0)$ represents the initial concentration before photolysis. The evolution of the isotopic ratio R which is defined as the ratio of c and c^* follows Eq(A6):

$$R(t) = \frac{c^*(t)}{c(t)} = \frac{c^*(0)}{c(0)}e^{-\int_0^t (J^* - J) dt} = R(0)e^{-\int_0^t (J^* - J) dt} \tag{A6}$$

Since the delta value $\delta^{15}N$ equals to $R_{spl}/R_{ref} - 1$ where R_{spl} and R_{ref} refer to the isotope ratio of sample and standard respectively, Eq(A6) can be further expanded to:

$$ln\frac{1+\delta(t)}{1+\delta(0)} = ln\frac{R(t)}{R(0)} = -\int_0^t (J^* - J)dt$$

$$= -\int_0^t J\varepsilon_p dt = -\bar{\varepsilon_p}\int_0^t Jdt = \bar{\varepsilon_p}ln(1-f_p) \qquad (A7)$$

which is consistent with the form of the Rayleigh equation.

By applying the first-order Taylor expansion of $ln(1+\delta^{15}N(NO_3^-)) \approx \delta^{15}N(NO_3^-)$, we obtain the relationship between the $\delta^{15}N(NO_3^-)$ before and after photolysis:

$$\delta^{15}N(SN_r) \approx \delta^{15}N(SN') - \bar{\varepsilon_p}ln(1-f_p) \qquad (A8)$$

The $\delta^{15}N$ of the emitted NO_2 can be calculate via the mass balance equation:

$$\delta^{15}N(SN') = (1-f_p)\delta^{15}N(SN_r) + f_p\delta^{15}N(NO_2) \qquad (A9)$$

Combining Eq(A8) and Eq(A9) would yield:

$$\delta^{15}N(NO_2) \approx \delta^{15}N(SN') + \frac{\bar{\varepsilon_p}(1-f_p)ln(1-f_p)}{f_p} \qquad (A10)$$

Because part of the photoproduct would undergo cage effect to reform nitrate (Fig A1), the final state of snow $\delta^{15}N(NO_3^-)$ after photolysis can be calculated via isotopic mass balance equation:

$$\delta^{15}N(SN) = \frac{(1-f_p)\delta^{15}N(SN_r) + f_c f_p \delta^{15}N(NO_2)}{1-f_p+f_c f_p}$$

$$= \delta^{15}N(SN') - \frac{(1-f_p)(1-f_c)\bar{\varepsilon_p}ln(1-f_p)}{(1-f_p)+f_c f_p} \qquad (A11)$$

which is equal to Eq (8).

~~The direct photolysis of snow nitrate obeys the Rayleigh equation with a nitrogen fractionation constant of $\bar{\varepsilon_p}$. The $\delta^{15}N$ of the photoproducts (NO_2) and the remaining nitrate on snow (SN_r) can be approximated by:~~

$$\delta^{15}N(NO_2) \approx \delta^{15}N(SN') + \frac{\bar{\varepsilon_p}(1-f_p)ln(1-f_p)}{f_p} \qquad (A2)$$

$$\delta^{15}N(SN_r) \approx \delta^{15}N(SN') - \bar{\varepsilon_p}ln(1-f_p) \qquad (A3)$$

~~Here we use the mathematic approximation of $ln(1+x) \sim x$. The $\delta^{15}N$ of the state after photolysis can be calculated via isotopic mass balance equation:~~

$$\delta^{15}N(SN) = \frac{(1-f_p)\delta^{15}N(SN_r) + f_cf_p\delta^{15}N(NO_2)}{1-f_p+f_cf_p}$$

$$= \delta^{15}N(SN') + \frac{(1-f_p)(1-f_c)\bar{\varepsilon}_p\ln(1-f_p)}{(1-f_p)+f_cf_p} \tag{A4}$$

which is equal to Eq (8).

For $\Delta^{17}O$, it is assumed that direct photolysis of nitrate will only induce mass-dependent fractionation and has no impact on $\Delta^{17}O$. However, the produced NO_2 which is re-oxidized by OH radical would lower its $\Delta^{17}O$ by 2/3 since OH radical would rapidly achieve isotopic equilibrium with the surrounding water molecule and erases its $\Delta^{17}O$ signal. Hence, by again using the isotopic mass balance equation, it can be shown that:

$$\Delta^{17}O(SN) = \frac{(1-f_p)\Delta^{17}O\left(SN'\right) + \frac{2}{3}f_cf_p\Delta^{17}O\left(SN'\right)}{1-f_p+f_cf_p}$$

$$= \frac{1-f_p+\frac{2}{3}f_cf_p}{1-f_p+f_cf_p}\Delta^{17}O\left(SN'\right) \tag{A5}$$

which is equal to Eq (9).
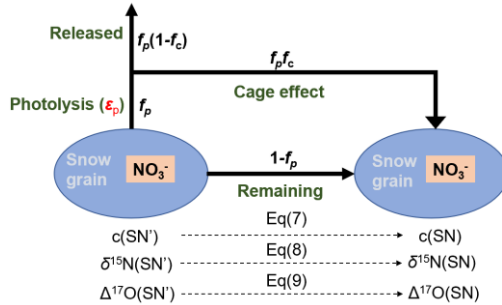
Figure A1. Sketch of the mass and isotopic transfer relationship during nitrate photolysis in snow grains. The black italic variables near the arrows indicate the fractional change in each subprocess.

Appendix B: method for calculating $\Delta^{17}O(NO_3^-)$ of FP

The $\Delta^{17}O(NO_3^-)$ of FP is required to solve the mass balance equations. We follow the algorithm for calculating atmospheric $\Delta^{17}O(NO_3^-)$ that has been widely used in previous study (Alexander et al., 2020). Atmospheric NO_2 is assumed to rapidly achieve photochemical steady state (PSS) so that its $\Delta^{17}O$ can be represented as follow:

$$\Delta^{17}O(NO_2) = \frac{k_{NO+O_3}[O_3] + k_{NO+BrO}[BrO]}{k_{NO+O_3}[O_3] + k_{NO+BrO}[BrO] + k_{NO+RO_2}[RO_2]}\Delta^{17}O(O_3^*) \quad \text{(B1)}$$

where k represents different oxidation channels for NO in the atmosphere and $\Delta^{17}O(O_3^*)$ represents $\Delta^{17}O$ of the terminal oxygen in the ozone molecule, RO_2 includes both HO_2 and other organic peroxyl radicals. Thus, to obtain $\Delta^{17}O(NO_2)$, concentrations of ozone and oxidizing radicals are necessary. For the subsequent oxidation of NO_2, only the NO_2+OH channel is considered, and $\Delta^{17}O$ of OH is assumed to be zero owing to its isotopic equilibrium with atmospheric H_2O. Thus, $\Delta^{17}O$ of the locally formed atmospheric nitrate (i.e., FP) can be calculated by:

$$\Delta^{17}O(NO_3^-) = \frac{2}{3}\Delta^{17}O(NO_2) \quad \text{(B2)}$$

Appendix C: adjusting the photolysis quantum yield used in Dome C simulations

The photolysis quantum yield (Φ) previously used in TRANSITS model simulation at Dome C was set to 0.026 in Erbland et al. (2015), which was adjusted to 0.015 in this study. Both values are obtained by best fitted the observed nitrate concentration and its $\delta^{15}N$ profiles in snowpack and are within the range of measurement results (0.003-0.44) for Dome C snow. However, using a value of 0.026 in the inverse model would severely overestimate the photolytic loss of snow nitrate, resulting unrealistically high nitrate concentration in the skin layer (>15000 ppb) and excessive fractionation in $\delta^{15}N(NO_3^-)$ (500 ‰) and $\Delta^{17}O(NO_3^-)$ (-18 ‰). Adjusting the quantum yield to 0.015 could well reproduce the observed nitrate concentration and $\delta^{15}N(NO_3^-)$ in skin layer and snowpack by the inverse model.

The discrepancy in the chosen quantum yield in these two models is caused by whether diffusion of snow nitrate is included, as the diffusion process would tend to smooth the entire snowpack nitrate profiles and decrease the asymptotic values. The omission of the diffusion process in the inverse model is based on the following considerations. First, the snowpack nitrate profile at sites with even lower accumulation rates (Dome A in East Antarctica, with annual snow accumulation rate of about 19 kg m^{-2} a^{-1}) does not display detectable a smoothing on snowpack nitrate or its $\delta^{15}N$ and $\Delta^{17}O$ (Shi et al., 2015), suggesting that diffusion is not as important as assumed in the

TRANSI~~S~~TS model. Second, the TRANSI~~S~~TS model would induce numerical diffusion during the division of snow layers in each time step, which results in rapidly decreases in the amplitude of the simulated seasonality in snow, as can be seen in the simulated snow profiles in Winton et al. (2020).

Appendix D: fitting the shape parameters for skin layer nitrate concentration at Dome C

To obtain a hypothetical seasonal pattern in the archived nitrate concentration, we assume that the normalized archived nitrate concentrations (by its arithmetic mean) would follow a same Gaussian-type distribution as nitrate concentrations in the skin layer, and the shape parameters (a, b, σ) are determined by using the least square regression method.
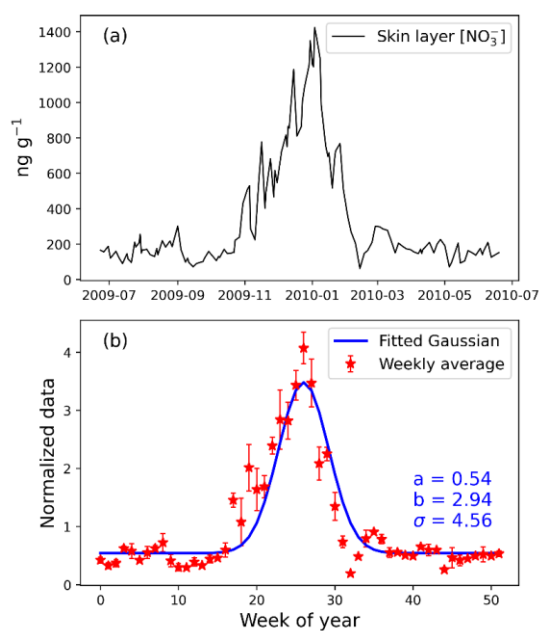
Figure D1. (a) Observed annual variations of skin layer nitrate concentration at Dome C (Erbland et al., 2013). **(b)** Normalized skin layer nitrate concentration by its arithmetic mean and the fitted Gaussian curve, with the shape parameters (a, b, σ) labeled in blue text.

Acknowledgements:

L.G. acknowledges financial support from the National Natural Science Foundation of China (Awards: 41822605 and 41871051) and the Strategic Priority Research Program of Chinese Academy of Sciences (XDB 41000000), and the National Key R&D Program of China (2022YFC3700701). This work was partially supported by the French national programme LEFE/INSU (IMAGO), the ANR grants ANR-15-IDEX-02 (project IDEX Université Grenoble Alpes) and Labex OSUG@2020 (Investissements d'avenir – ANR10 LABX56), the support of the overwintering staffs and the French polar institute IPEV through the SUNNITEDC (1011) and CAPOXI programs (1177) (J.S.). B. A. acknowledges support from NSF PLR 1542723 and AGS 2202287 and 1702266.

References

Abbatt, J. P. D.: Interaction of HNO$_3$ with water-ice surfaces at temperatures of the free troposphere, 24, 1479-1482, https://doi.org/10.1029/97GL01403, 1997.

Akers, P. D., Savarino, J., Caillon, N., Magand, O., and Le Meur, E.: Photolytic modification of seasonal nitrate isotope cycles in East Antarctica, Atmos. Chem. Phys., 22, 15637-15657, 10.5194/acp-22-15637-2022, 2022.

Akers, P. D., Savarino, J., Caillon, N., Servettaz, A. P. M., Le Meur, E., Magand, O., Martins, J., Agosta, C., Crockford, P., Kobayashi, K., Hattori, S., Curran, M., van Ommen, T., Jong, L., and Roberts, J. L.: Sunlight-driven nitrate loss records Antarctic surface mass balance, Nature Communications, 13, 4274, 10.1038/s41467-022-31855-7, 2022.

Alexander, B., Savarino, J., Kreutz, K. J., and Thiemens, M. H.: Impact of preindustrial biomass-burning emissions on the oxidation pathways of tropospheric sulfur and nitrogen, 109, https://doi.org/10.1029/2003JD004218, 2004.

Alexander, B., Sherwen, T., Holmes, C. D., Fisher, J. A., Chen, Q., Evans, M. J., and Kasibhatla, P.: Global inorganic nitrate production mechanisms: comparison of a global model with nitrate isotope observations, Atmos. Chem. Phys., 20, 3859-3877, 10.5194/acp-20-3859-2020, 2020.

Barbero, A., Savarino, J., Grilli, R., Blouzon, C., Picard, G., Frey, M. M., Huang, Y., and Caillon, N.: New Estimation of the NOx Snow-Source on the Antarctic Plateau, J. Geophys. Res., 126, e2021JD035062, https://doi.org/10.1029/2021JD035062, 2021.

Bennartz, R., Fell, F., Pettersen, C., Shupe, M. D., and Schuettemeyer, D.: Spatial and temporal variability of snowfall over Greenland from CloudSat observations, Atmos. Chem. Phys., 19, 8101-8121, 10.5194/acp-19-8101-2019, 2019.

Bergin, M. H., Jaffrezo, J.-L., Davidson, C. I., Dibb, J. E., Pandis, S. N., Hillamo, R., Maenhaut, W., Kuhns, H. D., and Makela, T.: The contributions of snow, fog, and dry deposition to the summer flux of anions and cations at Summit, Greenland, J. Geophys. Res., 100, 16275-16288, https://doi.org/10.1029/95JD01267, 1995.

Berhanu, T. A., Meusinger, C., Erbland, J., Jost, R., Bhattacharya, S. K., Johnson, M. S., and Savarino, J.: Laboratory study of nitrate photolysis in Antarctic snow. II. Isotopic effects and wavelength

940   dependence, 140, 244306, 10.1063/1.4882899, 2014.

Beyn, F., Matthias, V., and Dähnke, K.: Changes in atmospheric nitrate deposition in Germany – An isotopic perspective, Environmental Pollution, 194, 1-10, https://doi.org/10.1016/j.envpol.2014.06.043, 2014.

Burkhart, J. F., Hutterli, M., Bales, R. C., and McConnell, J. R.: Seasonal accumulation timing and

945   preservation of nitrate in firn at Summit, Greenland, Journal of Geophysical Research: Atmospheres, 109, 2004.

Caiazzo, L., Becagli, S., Bertinetti, S., Grotti, M., Nava, S., Severi, M., and Traversi, R.: High Resolution Chemical Stratigraphies of Atmospheric Depositions from a 4 m Depth Snow Pit at Dome C (East Antarctica), 12, 909, 2021.

950 Castellani, B. B., Shupe, M. D., Hudak, D. R., and Sheppard, B. E.: The annual cycle of snowfall at Summit, Greenland, 120, 6654-6668, https://doi.org/10.1002/2015JD023072, 2015.

Chu, L. and Anastasio, C.: Quantum Yields of Hydroxyl Radical and Nitrogen Dioxide from the Photolysis of Nitrate on Ice, The Journal of Physical Chemistry A, 107, 9594-9602, 10.1021/jp0349132, 2003.

955 Dibb, J. E., Talbot, R. W., Munger, J. W., Jacob, D. J., and Fan, S. M.: Air-snow exchange of HNO3 and NOy at Summit, Greenland, Journal of Geophysical Research: Atmospheres, 103, 3475-3486, doi.org/10.1029/97JD03132, 1998.

Dibb, J. E., Talbot, R. W., Whitlow, S. I., Shipham, M. C., Winterle, J., McConnell, J., and Bales, R.: Biomass burning signatures in the atmosphere and snow at Summit, Greenland: An event on 5

960   August 1994, Atmos. Environ., 30, 553-561, https://doi.org/10.1016/1352-2310(95)00328-2, 1996.

Dibb, J. E., Whitlow, S. I., and Arsenault, M.: Seasonal variations in the soluble ion content of snow at Summit. Greenland: Constraints from three years of daily surface snow samples, Atmos. Environ., 41, 5007-5019, https://doi.org/10.1016/j.atmosenv.2006.12.010, 2007.

Elliott, E. M., Yu, Z., Cole, A. S., and Coughlin, J. G.: Isotopic advances in understanding reactive

965   nitrogen deposition and atmospheric processing, Science of The Total Environment, 662, 393-403, https://doi.org/10.1016/j.scitotenv.2018.12.177, 2019.

Erbland, J., Savarino, J., Morin, S., France, J. L., Frey, M. M., and King, M. D.: Air–snow transfer of nitrate on the East Antarctic Plateau – Part 2: An isotopic model for the interpretation of deep ice-core records, Atmos. Chem. Phys., 15, 12079-12113, 10.5194/acp-15-12079-2015, 2015.

970 Erbland, J., Vicars, W. C., Savarino, J., Morin, S., Frey, M. M., Frosini, D., Vince, E., and Martins, J. M. F.: Air–snow transfer of nitrate on the East Antarctic Plateau – Part 1: Isotopic evidence for a photolytically driven dynamic equilibrium in summer, Atmos. Chem. Phys., 13, 6403-6419, 10.5194/acp-13-6403-2013, 2013.

Esquivel Hernández, G., Matiatos, I., Sánchez-Murillo, R., Balestrini, R., Wells, N., Monteiro, L.,

975   Chantara, S., Walters, W., and Wassenaar, L.: NITRATE ISOTOPES (δ15N, δ18O) IN PRECIPITATION: BEST PRACTICES FROM AN INTERNATIONAL COORDINATED RESEARCH PROJECT, 2022.

Fang, H., Walters, W. W., Mase, D., and Michalski, G.: iNRACM: incorporating 15N into the Regional Atmospheric Chemistry Mechanism (RACM) for assessing the role photochemistry plays in

980   controlling the isotopic composition of NOx, NOy, and atmospheric nitrate, Geosci. Model Dev., 14, 5001-5022, 10.5194/gmd-14-5001-2021, 2021.

Fibiger, D. L., Dibb, J. E., Chen, D., Thomas, J. L., Burkhart, J. F., Huey, L. G., and Hastings, M. G.: Analysis of nitrate in the snow and atmosphere at Summit, Greenland: Chemistry and transport, 121,

5010-5030, https://doi.org/10.1002/2015JD024187, 2016.

Fischer, H., Wagenbach, D., and Kipfstuhl, J.: Sulfate and nitrate firn concentrations on the Greenland ice sheet: 2. Temporal anthropogenic deposition changes, 103, 21935-21942, https://doi.org/10.1029/98JD01886, 1998.

Frey, M. M., Brough, N., France, J. L., Anderson, P. S., Traulle, O., King, M. D., Jones, A. E., Wolff, E. W., and Savarino, J.: The diurnal variability of atmospheric nitrogen oxides (NO and NO$_2$) above the Antarctic Plateau driven by atmospheric stability and snow emissions, Atmos. Chem. Phys., 13, 3045-3062, 10.5194/acp-13-3045-2013, 2013.

Frey, M. M., Roscoe, H. K., Kukui, A., Savarino, J., France, J. L., King, M. D., Legrand, M., and Preunkert, S.: Atmospheric nitrogen oxides (NO and NO$_2$) at Dome C, East Antarctica, during the OPALE campaign, Atmos. Chem. Phys., 15, 7859-7875, 10.5194/acp-15-7859-2015, 2015.

Frey, M. M., Savarino, J., Morin, S., Erbland, J., and Martins, J. M. F.: Photolysis imprint in the nitrate stable isotope signal in snow and atmosphere of East Antarctica and implications for reactive nitrogen cycling, Atmos. Chem. Phys., 9, 8681-8696, 10.5194/acp-9-8681-2009, 2009.

Freyer, H. D.: Seasonal variation of 15N/14N ratios in atmospheric nitrate species, Tellus B: Chemical and Physical Meteorology, 43, 30-44, 10.3402/tellusb.v43i1.15244, 1991.

Furukawa, R., Uemura, R., Fujita, K., Sjolte, J., Yoshimura, K., Matoba, S., and Iizuka, Y.: Seasonal-Scale Dating of a Shallow Ice Core From Greenland Using Oxygen Isotope Matching Between Data and Simulation, 122, 10,873-810,887, https://doi.org/10.1002/2017JD026716, 2017.

Gao, Y., Zhou, F., Ciais, P., Miao, C., Yang, T., Jia, Y., Zhou, X., Klaus, B.-B., Yang, T., and Yu, G.: Human activities aggravate nitrogen-deposition pollution to inland water over China, National science review, 7, 430-440, https://doi.org/10.1093/nsr/nwz073, National Science Review, 2019.

Geng, L., Alexander, B., Cole-Dai, J., Steig, E. J., Savarino, J., Sofen, E. D., and Schauer, A. J.: Nitrogen isotopes in ice core nitrate linked to anthropogenic atmospheric acidity change, 111, 5808-5812, https://doi:10.1073/pnas.1319441111, 2014.

Geng, L., Murray, L. T., Mickley, L. J., Lin, P., Fu, Q., Schauer, A. J., and Alexander, B.: Isotopic evidence of multiple controls on atmospheric oxidants over climate transitions, Nature, 546, 133-136, 10.1038/nature22340, 2017.

Geng, L., Zatko, M. C., Alexander, B., Fudge, T. J., Schauer, A. J., Murray, L. T., and Mickley, L. J.: Effects of post-depositional processing on nitrogen isotopes of nitrate in the Greenland Ice Sheet Project 2 ice core, 42, 5346-5354, https://doi.org/10.1002/2015GL064218, 2015.

Grisart, A., Casado, M., Gkinis, V., Vinther, B., Naveau, P., Vrac, M., Laepple, T., Minster, B., Prié, F., Stenni, B., Fourré, E., Steen-Larsen, H. C., Jouzel, J., Werner, M., Pol, K., Masson-Delmotte, V., Hoerhold, M., Popp, T., and Landais, A.: Sub-millennial climate variability from high-resolution water isotopes in the EPICA Dome C ice core, Clim. Past, 18, 2289-2301, 10.5194/cp-18-2289-2022, 2022.

Hastings, M. G., Steig, E. J., and Sigman, D. M.: Seasonal variations in N and O isotopes of nitrate in snow at Summit, Greenland: Implications for the study of nitrate in snow and ice cores, 109, https://doi.org/10.1029/2004JD004991, 2004.

Heaton, T. H. E.: 15N14N ratios of nitrate and ammonium in rain at Pretoria, South Africa, Atmospheric Environment (1967), 21, 843-852, https://doi.org/10.1016/0004-6981(87)90080-1, 1987.

Holland, E. A., Dentener, F. J., Braswell, B. H., and Sulzman, J. M.: Contemporary and Pre-Industrial Global Reactive Nitrogen Budgets, Biogeochemistry, 46, 7-43, 1999.

Honrath, R., Lu, Y., Peterson, M. C., Dibb, J. E., Arsenault, M., Cullen, N., and Steffen, K. J. A. E.: Vertical fluxes of NOx, HONO, and HNO3 above the snowpack at Summit, Greenland, 36, 2629-2640, 2002.

Iizuka, Y., Uemura, R., Fujita, K., Hattori, S., Seki, O., Miyamoto, C., Suzuki, T., Yoshida, N., Motoyama, H., and Matoba, S.: A 60 Year Record of Atmospheric Aerosol Depositions Preserved in a High-Accumulation Dome Ice Core, Southeast Greenland, 123, 574-589, https://doi.org/10.1002/2017JD026733, 2018.

Ishino, S., Hattori, S., Savarino, J., Jourdain, B., Preunkert, S., Legrand, M., Caillon, N., Barbero, A., Kuribayashi, K., and Yoshida, N.: Seasonal variations of triple oxygen isotopic compositions of atmospheric sulfate, nitrate, and ozone at Dumont d'Urville, coastal Antarctica, Atmos. Chem. Phys., 17, 3713-3727, 10.5194/acp-17-3713-2017, 2017.

Jaffrezo, J.-L., Davidson, C. I., Kuhns, H. D., Bergin, M. H., Hillamo, R., Maenhaut, W., Kahl, J. W., and Harris, J. M.: Biomass burning signatures in the atmosphere of central Greenland, 103, 31067-31078, https://doi.org/10.1029/98JD02241, 1998.

Jiang, Z., Alexander, B., Savarino, J., Erbland, J., and Geng, L.: Impacts of the photo-driven post-depositional processing on snow nitrate and its isotopes at Summit, Greenland: a model-based study, The Cryosphere, 15, 4207-4220, 2021.

Jiang, Z., Savarino, J., Alexander, B., Erbland, J., Jaffrezo, J. L., and Geng, L.: Impacts of post-depositional processing on nitrate isotopes in the snow and the overlying atmosphere at Summit, Greenland, The Cryosphere, 16, 2709-2724, 10.5194/tc-16-2709-2022, 2022.

Kahl, J. D. W., Martinez, D. A., Kuhns, H., Davidson, C. I., Jaffrezo, J.-L., and Harris, J. M.: Air mass trajectories to Summit, Greenland: A 44-year climatology and some episodic events, 102, 26861-26875, https://doi.org/10.1029/97JC00296, 1997.

Kaufmann, P. R., Federer, U., Hutterli, M. A., Bigler, M., Schüpbach, S., Ruth, U., Schmitt, J., and Stocker, T. F.: An Improved Continuous Flow Analysis System for High-Resolution Field Measurements on Ice Cores, Environmental Science & Technology, 42, 8044-8050, 10.1021/es8007722, 2008.

Krankowsky, D., Lämmerzahl, P., and Mauersberger, K.: Isotopic measurements of stratospheric ozone, 27, 2593-2595, https://doi.org/10.1029/2000GL011812, 2000.

Kunasek, S. A., Alexander, B., Steig, E. J., Hastings, M. G., Gleason, D. J., and Jarvis, J. C.: Measurements and modeling of $\Delta17O$ of nitrate in snowpits from Summit, Greenland, 113, https://doi.org/10.1029/2008JD010103, 2008.

Lämmerzahl, P., Röckmann, T., Brenninkmeijer, C. A. M., Krankowsky, D., and Mauersberger, K.: Oxygen isotope composition of stratospheric carbon dioxide, 29, 23-21-23-24, https://doi.org/10.1029/2001GL014343, 2002.

Lee, H.-M., Henze, D. K., Alexander, B., and Murray, L. T.: Investigating the sensitivity of surface-level nitrate seasonality in Antarctica to primary sources using a global model, Atmos. Environ., 89, 757-767, https://doi.org/10.1016/j.atmosenv.2014.03.003, 2014.

Legrand, M. R. and Delmas, R. J.: Relative contributions of tropospheric and stratospheric sources to nitrate in Antarctic snow, Tellus B: Chemical and Physical Meteorology, 38, 236-249, 10.3402/tellusb.v38i3-4.15132, 1986.

Levy II, H., Moxim, W. J., Klonecki, A. A., and Kasibhatla, P. S.: Simulated tropospheric NO x : Its evaluation, global distribution and individual source contributions, 104, 26279-26306, https://doi.org/10.1029/1999JD900442, 1999.

Li, J., Davy, P., Harvey, M., Katzman, T., Mitchell, T., and Michalski, G.: Nitrogen isotopes in nitrate aerosols collected in the remote marine boundary layer: Implications for nitrogen isotopic fractionations among atmospheric reactive nitrogen species, Atmos. Environ., 245, 118028, https://doi.org/10.1016/j.atmosenv.2020.118028, 2021.

Li, J., Zhang, X., Orlando, J., Tyndall, G., and Michalski, G.: Quantifying the nitrogen isotope effects during photochemical equilibrium between NO and NO2: implications for $\delta^{15}N$ in tropospheric reactive nitrogen, Atmos. Chem. Phys., 20, 9805-9819, 10.5194/acp-20-9805-2020, 2020.

Li, Y., Shi, G., Chen, Z., Lan, M., Ding, M., Li, Z., and Hastings, M. G.: Significant Latitudinal Gradient of Nitrate Production in the Marine Atmospheric Boundary Layer of the Northern Hemisphere, 49, e2022GL100503, https://doi.org/10.1029/2022GL100503, 2022.

Lim, S., Lee, M., Savarino, J., and Laj, P.: Oxidation pathways and emission sources of atmospheric particulate nitrate in Seoul: based on $\delta^{15}N$ and $\Delta^{17}O$ measurements, Atmos. Chem. Phys., 22, 5099-5115, 10.5194/acp-22-5099-2022, 2022.

Lyons, J. R.: Transfer of mass-independent fractionation in ozone to other oxygen-containing radicals in the atmosphere, 28, 3231-3234, https://doi.org/10.1029/2000GL012791, 2001.

Madronich, S., McKenzie, R. L., Björn, L. O., and Caldwell, M. M.: Changes in biologically active ultraviolet radiation reaching the Earth's surface, Journal of Photochemistry and Photobiology B: Biology, 46, 5-19, https://doi.org/10.1016/S1011-1344(98)00182-1, 1998.

Mauersberger, K., Krankowsky, D., and Janssen, C.: Oxygen Isotope Processes and Transfer Reactions, Space Science Reviews, 106, 265-279, 10.1023/A:1024650007258, 2003.

McCabe, J. R., Boxe, C. S., Colussi, A. J., Hoffmann, M. R., and Thiemens, M. H.: Oxygen isotopic fractionation in the photochemistry of nitrate in water and ice, 110, https://doi.org/10.1029/2004JD005484, 2005.

Meusinger, C., Berhanu, T. A., Erbland, J., Savarino, J., and Johnson, M. S.: Laboratory study of nitrate photolysis in Antarctic snow. I. Observed quantum yield, domain of photolysis, and secondary chemistry, 140, 244305, 10.1063/1.4882898, 2014.

Morin, S., Erbland, J., Savarino, J., Domine, F., Bock, J., Friess, U., Jacobi, H.-W., Sihler, H., and Martins, J. M. F.: An isotopic view on the connection between photolytic emissions of NOx from the Arctic snowpack and its oxidation by reactive halogens, J. Geophys. Res., 117, https://doi.org/10.1029/2011JD016618, 2012.

Morin, S., Savarino, J., Frey, M. M., Domine, F., Jacobi, H.-W., Kaleschke, L., and Martins, J. M. F.: Comprehensive isotopic composition of atmospheric nitrate in the Atlantic Ocean boundary layer from 65°S to 79°N, J. Geophys. Res., 114, https://doi.org/10.1029/2008JD010696, 2009.

Morin, S., Savarino, J., Frey, M. M., Yan, N., Bekki, S., Bottenheim, J. W., and Martins, J. M. F.: Tracing the Origin and Fate of NO$_x$ in the Arctic Atmosphere Using Stable Isotopes in Nitrate, 322, 730-732, doi:10.1126/science.1161910, 2008.

Murray, L. T., Leibensperger, E. M., Orbe, C., Mickley, L. J., and Sulprizio, M.: GCAP 2.0: a global 3-D chemical-transport model framework for past, present, and future climate scenarios, Geosci. Model Dev., 14, 5789-5823, 10.5194/gmd-14-5789-2021, 2021.

Murray, L. T., Mickley, L. J., Kaplan, J. O., Sofen, E. D., Pfeiffer, M., and Alexander, B.: Factors controlling variability in the oxidative capacity of the troposphere since the Last Glacial Maximum, Atmos. Chem. Phys., 14, 3589-3622, 10.5194/acp-14-3589-2014, 2014.

Muscari, G., de Zafra, R. L., and Smyshlyaev, S.: Evolution of the NOy-N2O correlation in the Antarctic stratosphere during 1993 and 1995, 108, https://doi.org/10.1029/2002JD002871, 2003.

Pilegaard, K., Skiba, U., Ambus, P., Beier, C., Brüggemann, N., Butterbach-Bahl, K., Dick, J., Dorsey, J., Duyzer, J., Gallagher, M., Gasche, R., Horvath, L., Kitzler, B., Leip, A., Pihlatie, M. K., Rosenkranz, P., Seufert, G., Vesala, T., Westrate, H., and Zechmeister-Boltenstern, S.: Factors controlling regional differences in forest soil emission of nitrogen oxides (NO and N$_2$O), Biogeosciences, 3, 651-661, 10.5194/bg-3-651-2006, 2006.

Quinn, P. K., Shaw, G., Andrews, E., Dutton, E. G., Ruoho-Airola, T., and Gong, S. L.: Arctic haze: current trends and knowledge gaps, 59, 99-114, https://doi.org/10.1111/j.1600-0889.2006.00238.x, 2007.

Röthlisberger, R., Hutterli, M. A., Sommer, S., Wolff, E. W., and Mulvaney, R.: Factors controlling nitrate in ice cores: Evidence from the Dome C deep ice core, 105, 20565-20572, https://doi.org/10.1029/2000JD900264, 2000.

Savarino, J., Bhattacharya, S. K., Morin, S., Baroni, M., and Doussin, J.-F.: The NO+O3 reaction: A triple oxygen isotope perspective on the reaction dynamics and atmospheric implications for the transfer of the ozone isotope anomaly, 128, 194303, 10.1063/1.2917581, 2008.

Savarino, J., Kaiser, J., Morin, S., Sigman, D. M., and Thiemens, M. H.: Nitrogen and oxygen isotopic constraints on the origin of atmospheric nitrate in coastal Antarctica, Atmos. Chem. Phys., 7, 1925-1945, 10.5194/acp-7-1925-2007, 2007.

Savarino, J., Vicars, W. C., Legrand, M., Preunkert, S., Jourdain, B., Frey, M. M., Kukui, A., Caillon, N., and Gil Roca, J.: Oxygen isotope mass balance of atmospheric nitrate at Dome C, East Antarctica, during the OPALE campaign, Atmos. Chem. Phys., 16, 2659-2673, 10.5194/acp-16-2659-2016, 2016.

Seinfeld, J. H., Pandis, S. N. J. A. c., and physics: From air pollution to climate change, 1326, 1998.

Shi, G., Buffen, A. M., Hastings, M. G., Li, C., Ma, H., Li, Y., Sun, B., An, C., and Jiang, S.: Investigation of post-depositional processing of nitrate in East Antarctic snow: isotopic constraints on photolytic loss, re-oxidation, and source inputs, Atmos. Chem. Phys., 15, 9435-9453, 10.5194/acp-15-9435-2015, 2015.

Shi, G., Buffen, A. M., Hu, Y., Chai, J., Li, Y., Wang, D., and Hastings, M. G.: Modeling the Complete Nitrogen and Oxygen Isotopic Imprint of Nitrate Photolysis in Snow, 50, e2023GL103778, https://doi.org/10.1029/2023GL103778, 2023.

Shi, G., Buffen, A. M., Ma, H., Hu, Z., Sun, B., Li, C., Yu, J., Ma, T., An, C., Jiang, S., Li, Y., and Hastings, M. G.: Distinguishing summertime atmospheric production of nitrate across the East Antarctic Ice Sheet, Geochimica et Cosmochimica Acta, 231, 1-14, https://doi.org/10.1016/j.gca.2018.03.025, 2018.

Shi, G., Li, C., Li, Y., Chen, Z., Ding, M., Ma, H., Jiang, S., An, C., Guo, J., Sun, B., and Hastings, M. G.: Isotopic constraints on sources, production, and phase partitioning for nitrate in the atmosphere and snowfall in coastal East Antarctica, Earth and Planetary Science Letters, 578, 117300, https://doi.org/10.1016/j.epsl.2021.117300, 2022.

Shi, G., Ma, H., Zhu, Z., Hu, Z., Chen, Z., Jiang, S., An, C., Yu, J., Ma, T., Li, Y., Sun, B., and Hastings, M. G.: Using stable isotopes to distinguish atmospheric nitrate production and its contribution to the surface ocean across hemispheres, Earth and Planetary Science Letters, 564, 116914, https://doi.org/10.1016/j.epsl.2021.116914, 2021.

Sillman, S.: The relation between ozone, NOx and hydrocarbons in urban and polluted rural environments, Atmos. Environ., 33, 1821-1845, https://doi.org/10.1016/S1352-2310(98)00345-8, 1999.

Sofen, E. D., Alexander, B., Steig, E. J., Thiemens, M. H., Kunasek, S. A., Amos, H. M., Schauer, A. J., Hastings, M. G., Bautista, J., Jackson, T. L., Vogel, L. E., McConnell, J. R., Pasteris, D. R., and Saltzman, E. S.: WAIS Divide ice core suggests sustained changes in the atmospheric formation pathways of sulfate and nitrate since the 19th century in the extratropical Southern Hemisphere, Atmos. Chem. Phys., 14, 5749-5769, 10.5194/acp-14-5749-2014, 2014.

VanCuren, R. A., Cahill, T., Burkhart, J., Barnes, D., Zhao, Y., Perry, K., Cliff, S., and McConnell, J. J. A. e.: Aerosols and their sources at Summit Greenland–First results of continuous size-and time-resolved sampling, 52, 82-97, 2012.

Vicars, W. C. and Savarino, J.: Quantitative constraints on the 17O-excess ($\Delta17O$) signature of surface ozone: Ambient measurements from 50°N to 50°S using the nitrite-coated filter technique, Geochimica et Cosmochimica Acta, 135, 270-287, https://doi.org/10.1016/j.gca.2014.03.023, 2014.

Walters, W. W., Michalski, G., Böhlke, J. K., Alexander, B., Savarino, J., and Thiemens, M. H.: Assessing the Seasonal Dynamics of Nitrate and Sulfate Aerosols at the South Pole Utilizing Stable Isotopes, 124, 8161-8177, https://doi.org/10.1029/2019JD030517, 2019.

Winton, V. H. L., Ming, A., Caillon, N., Hauge, L., Jones, A. E., Savarino, J., Yang, X., and Frey, M. M.: Deposition, recycling, and archival of nitrate stable isotopes between the air–snow interface: comparison between Dronning Maud Land and Dome C, Antarctica, Atmos. Chem. Phys., 20, 5861-5885, 10.5194/acp-20-5861-2020, 2020.

Wolff, E. W., Jones, A. E., Bauguitte, S. J. B., and Salmon, R. A.: The interpretation of spikes and trends in concentration of nitrate in polar ice cores, based on evidence from snow and atmospheric measurements, Atmos. Chem. Phys., 8, 5627-5634, 10.5194/acp-8-5627-2008, 2008.

Wolff, E. W.: Nitrate in Polar Ice, Ice Core Studies of Global Biogeochemical Cycles, Berlin, Heidelberg, 195-224, doi.org/10.1007/978-3-642-51172-1_10,

Yang, Q., Mayewski, P. A., Whitlow, S., Twickler, M., Morrison, M., Talbot, R., Dibb, J., and Linder, E.: Global perspective of nitrate flux in ice cores, 100, 5113-5121, https://doi.org/10.1029/94JD03115, 1995.

Young, P. J., Archibald, A. T., Bowman, K. W., Lamarque, J. F., Naik, V., Stevenson, D. S., Tilmes, S., Voulgarakis, A., Wild, O., Bergmann, D., Cameron-Smith, P., Cionni, I., Collins, W. J., Dalsøren, S. B., Doherty, R. M., Eyring, V., Faluvegi, G., Horowitz, L. W., Josse, B., Lee, Y. H., MacKenzie, I. A., Nagashima, T., Plummer, D. A., Righi, M., Rumbold, S. T., Skeie, R. B., Shindell, D. T., Strode, S. A., Sudo, K., Szopa, S., and Zeng, G.: Pre-industrial to end 21st century projections of tropospheric ozone from the Atmospheric Chemistry and Climate Model Intercomparison Project (ACCMIP), Atmos. Chem. Phys., 13, 2063-2090, 10.5194/acp-13-2063-2013, 2013.

Zatko, M. C., Grenfell, T. C., Alexander, B., Doherty, S. J., Thomas, J. L., and Yang, X.: The influence of snow grain size and impurities on the vertical profiles of actinic flux and associated NO_x emissions on the Antarctic and Greenland ice sheets, Atmos. Chem. Phys., 13, 3547-3567, 10.5194/acp-13-3547-2013, 2013.

Zatko, M., Erbland, J., Savarino, J., Geng, L., Easley, L., Schauer, A., Bates, T., Quinn, P. K., Light, B., Morison, D., Osthoff, H. D., Lyman, S., Neff, W., Yuan, B., and Alexander, B.: The magnitude of the snow-sourced reactive nitrogen flux to the boundary layer in the Uintah Basin, Utah, USA, Atmos. Chem. Phys., 16, 13837-13851, 10.5194/acp-16-13837-2016, 2016.

Zhang, L., Jacob, D. J., Knipping, E. M., Kumar, N., Munger, J. W., Carouge, C. C., van Donkelaar, A., Wang, Y. X., and Chen, D.: Nitrogen deposition to the United States: distribution, sources, and processes, Atmos. Chem. Phys., 12, 4539-4554, 10.5194/acp-12-4539-2012, 2012.